Shahrood University of Technology

Iranian Society of Mining Engineering (IRSME)

Journal of Mining and Environment (JME)

journal homepage: www.jme.shahroodut.ac.ir

THOMSON REUTERS

Application of Fuzzy Gamma Operator to Generate Mineral Prospectivity Mapping for Cu-Mo Porphyry Deposits (Case Study: Kighal-Bourmolk Area, Northwestern Iran)

Masoud Esmailzadeh[1], Ali Imamalipour[1*] and Farhang Aliyari[2]

1- Department of Mining Engineering, Urmia University, Urmia, Iran
2- Department of Mining Engineering, Urmia University of Technology, Urmia, Iran

Article Info

Received 20 September 2021
Received in Revised form 29 January 2022
Accepted 7 March 2022
Published online 7 March 2022

DOI:10.22044/jme.2022.11218.2103

Keywords

Mineral prospectivity mapping
Cu-Mo porphyry
Fuzzy gamma operator
Mineralization
Kighal-Bourmolk

Abstract

The main aim of mineral exploration is to discover the ore deposits. The mineral prospectivity mapping (MPM) methods by employing multi-criteria decision-making (MCDM) integrate the exploration layers. This research work combines the geological, alteration, and geochemical data in order to generate MPM in the Kighal-Bourmolk Cu-Mo porphyry deposit. The overlaying of rock units and fault layers was used to prepare the geological layer. The remote sensing and geological studies were employed in order to create an alteration layer. For generating the geo-chemistry layer, the stream sediment and lithogeochemical data were utilized. The lithogeochemistry layer was categorized into 9 ones including Cu, Mo, Bi, Te, the alteration indices (e.g. potassic, phyllic, and propylitic), and the geochemical zonality indices (e.g. Vz1 and Vz2). In addition, the stream sediment layer was categorized into 6 layers including Cu, Mo, Bi, Te, and the geochemical zonality indices (e.g. Vz1 and Vz2). By examination of the created layers, the consistency of the potential areas was verified by field surveys. Afterward, the weights were assigned to each layer considering the conceptual model of porphyry copper systems. Consequently, the layers were integrated by the fuzzy gamma operator technique, and the final MPM was generated. Regarding the generated MPM, 0.86% of the studied area shows a high potential porphyry mineralization, and these areas are proposed for the subsequent exploration drilling locations.

1. Introduction

The purpose of Mineral Prospectivity Mapping (MPM) is to explore the novel economical depositions in a region of interest. This procedure utilizes the geospatial datasets (e.g. geological, geochemical, remote sensing) simultaneously. Hence, MPM is a multiple criterion decision-making (MCDM) task that prepares a predictive model for prioritizing the mineralized zones in the region of interest [1-2].

Knowledge-driven and data-driven are the two major techniques for providing MPM, and identify the high potential zones for the aimed deposit [3-4]. The theory of fuzzy logic [5], which is categorized in the knowledge-driven group, is one of the well-known MPM approaches. This technique requires experience and expert geo-scientist decision-makers (GDMs) to define the fuzzy scores [6-7]. Using the fuzzy logic to simulate MPM has been in the center of focus by several investigations [8- 6- 2].

As represented by Carranza (2014) [4], the knowledge-driven approach is utilized in order to create the predictive modeling of MPM in the intact and undiscovered areas (or so-called "greenfield" areas) to discern the promising areas as well as determination of the boreholes points including the Boolean logic and index overlay methods [9], fuzzy logic overlay [10-11], fuzzy inference system [12-13-6]. Simultaneously, the data-driven algorithm is used to prepare the

Corresponding author: a.imamalipour@urmia.ac.ir (A. Imamalipour).

predictive modeling of MPM in the entirely sampled and known areas (or so-called "brownfield") in order to diagnose the exact and more exploration areas by the usage of information from the pre-explored or extracted areas. This information is used as the "training data" for determining the spatial relationships between the specific geological, geo-chemical, and geophysical characteristics such as the favorability analysis [14], neural networks [15-16], discriminant analysis [17], weights of evidence [18], evidential belief functions [19], logistic regression [20], fractal-based outranking approach [21], analytical hierarchical prospectivity mapping [22], and multifractal modeling [23].

As described by Jackson (2010) [24], the geo-chemical zonation is one of the prominent and beneficial concepts in the exploration investigations that utilizes the primary haloes patterns in the studies. Most economic deposits are zoned mineralogically and geo-chemically [25-26]. The zonality is an effective technique in prediction for the erosion level of mineralization and discerning of the sub-ore and supra-ore primary haloes as well as exploration of the blind mineral deposits [27-28- 24-29-30]. Numerous exploration operations have been focused in the form of various projects in different areas of the Azerbaijan region due to its long and complex geological and structural evolution and metallogenic history [31-32-33]. However, despite the abundant successful mineral exploration and mining developments, the overall potential of the Azerbaijan region for precious and base metal deposits has not been fully understood.

The studied area is located in the Ahar-Arasbaran Metallogenic Zone (AAMZ), called Kighal-Bourmolk (KB). The main aim of this work is to integrate the predictive layers consisting of the geological, remote sensing, and geo-chemistry by the fuzzy logic approach to explore the Cu-Mo porphyry system. The innovation of this work is to apply the surface erosion layers (sub-branches in geo-chemical layers). This area has enough data to study in this case, so the results can be accepted for further studies. The generated MPM of KB by fuzzy logic led to identifying the high potential zone in the eastern part of the area. In the following, considering the zonality studies, the central part of the deposit has an outcrop on the surface, and the western part of the area has the maximum level of erosion.

2. Geological Setting

The KB area is located in the Central Iran zone and the Alborz-Azerbaijan zone according to the geological-structural classification of Stocklin (1968) [34] and Nabavi (1976) [35], respectively. The KB area is located in the Arasbaran metallogenic zone, which forms the middle part of the Alborz-Arasbaran-Lesser Caucasus magmatic belt. The Arasbaran metallogenic zone includes the areas to the north of Meshkin Shahr, Ahar, Kalibar, Varzeghan, Siah Rud, Arasbaran, and Qareh Dagh Hills. This metallogenic zone is bordered on the south-southwest by the Tabriz-Soltanieh fault, on the east by the Ardebil-Mianeh fault, and on the north-east by the embayment near the east-west trending Moghan fault.

In this zone, the Upper Cretaceous magmatic rocks consist of basic-intermediate submarine volcanic rocks [36]. The following Eocene volcanic activity commenced with the eruption of alkaline rocks and terminated with the subordinate felsic components [37-38], followed by multi-stage, acid to intermediate (with minor basic) intrusions. During the Late Eocene-Early Oligocene, the tectonic activities associated with the emplacement of plutonic bodies were dominant [39]. Regionally, an intensive phase of igneous activity began in the Late Oligocene-Early Miocene, initially in the form of andesitic, trachytic-andesitic, trachytic, and occasionally rhyolitic volcanism. This magmatism continued until the Late Miocene [37]. Several small sub-volcanic bodies of porphyric quartz-monzonite to monzodiorite were also emplaced. Porphyry, skarn, and intrusion-related types of Cu-Mo mineralization are associated with this magmatism at several deposits consisting of the Sungun, Haftcheshmeh, Mivehrud, Kigal, Niaz, Saheb Divan, Shelehboran, Masjeddaghi, and Mazraeh [36-37-38-25]. These deposits were formed during the intrusion of quartz-monzonite-granodiorite-diorite porphyry stocks into the Upper Cretaceous-Eocene andesitic volcano-sedimentary sequences [36].

The mineralization stages in AAMZ consist of (a) Upper Oligocene to Lower Miocene (~20 Ma), Cu-Mo porphyry mineralization, and (b) Upper Miocene (~10 Ma) Cu-Au porphyry and epithermal Cu-Au mineralization [37].

Based upon the field observations and the geochronological data, at least two major intrusion cycles were distinguished in the Tertiary magmatism of AAMZ [36-38-37]. The cycle-I intrusions are mainly composed of granodiorite, granite, syenite, and quartz-diorite with alkaline to shoshonitic affinities such as Ordubad and Sheivardagh batholiths. The cycle-II magmatism consists of sub-volcanic bodies of quartz-monzonite to monzodiorite. These stocks have porphyritic textures, and are commonly calc-alkaline with adakitic affinity.

Porphyry, skarn, and intrusion-related types of Cu-Mo-Au mineralization are associated with the cycle-II porphyry stocks in the Sungun, Haftcheshmeh, Mivehrud, Kajaran, Annigh-Gharehchilar, Kighal, Masjeddaghi, and Mazraeh [36-38-37].

Based on the 1:100,000 geological map of Varzeghan and the 1:25000 geological map of the KB area [40], the rock units of KB include the upper Eocene acidic to intermediate volcanic and pyroclastic rocks ranging in composition from andesite, trachyandesite, dacite, tuff, agglomerate, and rhyolite. These units are intruded by the granodiorite and monzonite porphyry intrusions. The propylitic, argillic, phyllic, potassic, and silica hydrothermal alteration zones and associated Cu–Mo porphyry mineralization are developed in the KB area. The late Oligocene–early Miocene age (20.1 ± 1.8 Ma) of the Kighal porphyry stock has been confirmed by the Ar-Ar geochronological dating [36].

According to KCE (2006) [40], the faults in the KB area are generally characterized by a high angel to vertical strike-slip faults that can be divided into four groups in the term of strike and spatial orientation (Figure 1):

i. The N60W-N25W-trending faults with nearly vertical strike-slip faults. These faults are represented by a sinistral displacement.

ii. The S80W-N70W-trending faults with generally vertical dip to a negligible displacement along strike that has the same strike with the youngest dikes of the area.

iii. The S70W-S25W-striking faults have the same directions as the young dikes. These faults are significantly associated with the hydrothermal alteration and the Cu-Mo-Au mineralization.

iv. The north-south-striking dextral faults are distinguished by a considerable long but minor displacement along strike.

3. Application and methodology of study in Kighal-Bourmolk deposit

The remote sensing, geochemical, and lithological geo-data sets were applied, and evidential layers were generated to recognize the high potential and prospectivity mapping in the KB deposit. The generating procedure of the layers are as follows:

3.1. Remote sensing layers

The Advanced Spaceborne Thermal Emission and Reflection Radiometer (ASTER) spectral images were implemented in order to generate the remote sensing layer. The pre-processing approaches such as the geometric and radiometric corrections were conducted before processing the ASTER images. The selected band numbers that were used in this work are 1 to 9.

Based on the conceptual model of porphyry deposits [41], the main alterations associated with these deposits encompass the potassic, phyllic, argillic, and propylitic zones. In this work, the implemented techniques used to distinguish the mentioned alterations were image-based (RGB, Band ratio; PCA, Principal Component Analysis, and Crosta-PCA) and spectral-based (SAM; Spectral Angle Mapper).

Processing on the satellite images to extract information by combining bands is called False Color Composite (FCC). This combining is useful in order to identify the alternation minerals [42]. The other simple and powerful method in remote sensing is band rationing. Theoretically, band rationing is beneficial for highlighting or overstating the anomaly of the interested area [43]. This method is also decreasing the effect of topography, and therefore, it reinforces the variations among the spectral reflexes of each band [44]. The other approach used in this work was Principal Component Analysis (PCA). As presented by Alavi Panah (2003) [45], the most important application of PCA is to take information from two or more channels, and decrease the number of channels for a well and simple image processing. The analysis of the main components is a linear transmission that rotates linear axes throughout the image space in the maximum variance. The rotation is based on the special vectors of the covariance matrix, which is made up of the input data. In the PCA method, the information of several images is compressed into one image, and the difference in brightness is maximized. The number of PCAs made depends on the number of selected bands. During the selecting bands to apply the PCA algorithm, less correlated bands should be selected because the lower the correlation of the bands, the more information their composition will contain [46]. The selective principal component analysis or the Crosta-PCA method is similar to the PCA method but it uses a smaller number of bands to identify and classify the alteration zones, and also it will provide more reliable results than the PCA method. The procedure of remote sensing processing of the KB area is briefly presented in Table 1 and Figures 2a-h.

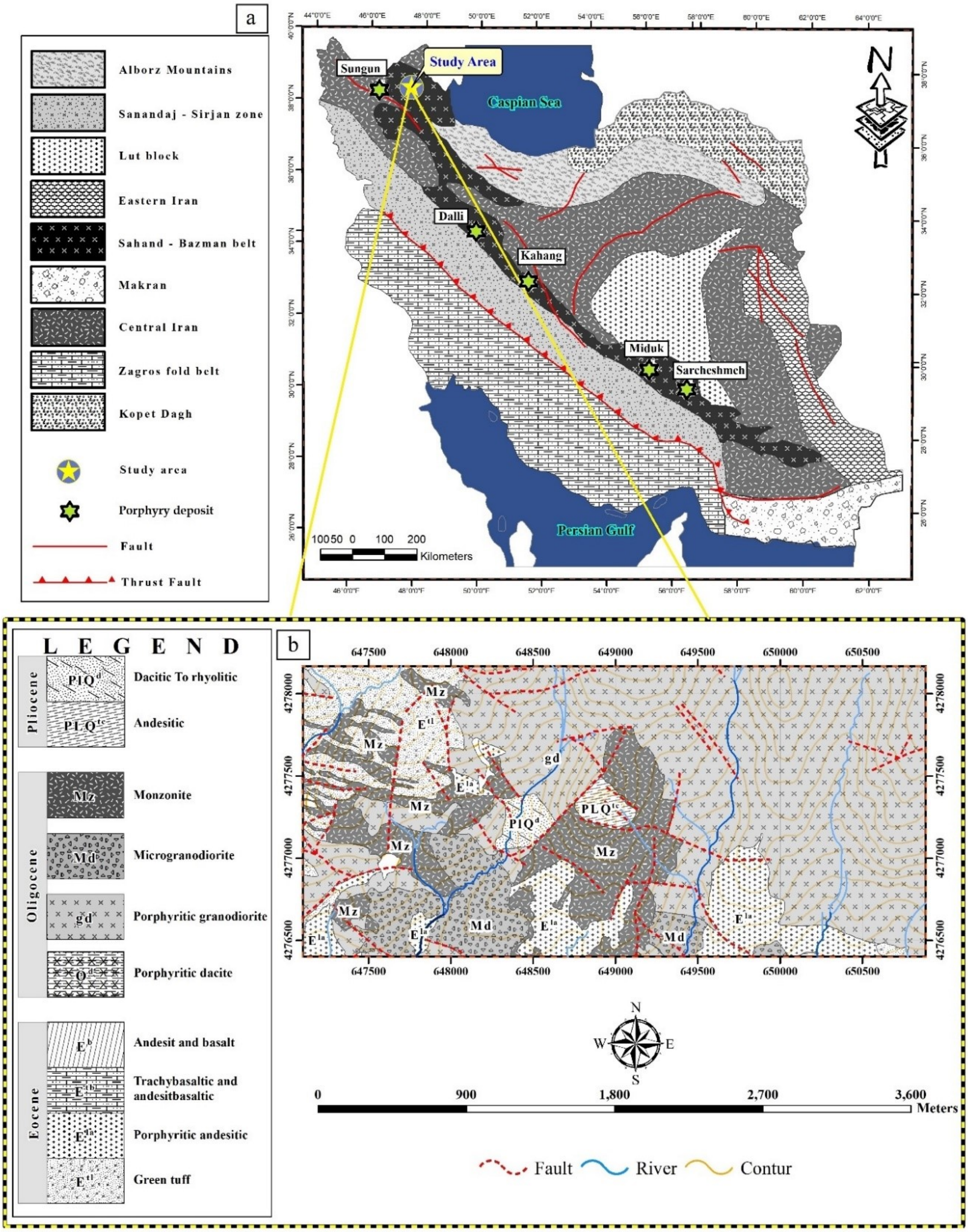

Figure 1. (a) A simplified structural map of Iran showing major structural units and location of studied area. (b) detailed geological map of KB [40].

Table 1. Process of remote sensing in area under study.

Image-based

Method	Alternation	False color composite	Figure	Color of alternation area in map	Description
RGB	Phyllic	RGB (468)	(Fig. 3a)	Pink	Alterations are quite visible in middle parts and especially near KB village.
	Argillic	RGB (468)	(Fig. 3a)	Pink	
	Propylitic	RGB (468)	(Fig. 3a)	Green	

Method	Alternation	Used mineral	Band ratio	Figure	Color of alternation area on map
Band Ratio	Phyllic	Sericite	$\frac{Band\ 7}{Band\ 6}$	(Fig. 3b)	Light pixels
	Argillic	Kaolinite	$\frac{Band\ 6}{Band\ 5}$	(Fig. 3c)	Light pixels
	Propylitic	Chlorite	$\frac{Band\ 9}{Band\ 8}$	(Fig. 3d)	Light pixels

Method	Alternation	False-color composite	Figure	Color of alternation area in map
RGB-Band Ratio	Phyllic	RGB (9/8, 7/6, 6/5)	(Fig. 3e)	Yellow
	Argillic	RGB (9/8, 7/6, 6/5)	(Fig. 3e)	Yellow
	Propylitic	RGB (9/8, 7/6, 6/5)	(Fig. 3e)	Green

Method	Alternation	Used mineral and bands	PCA (Eigenvector)					Description
PCA (Crosta)	Phyllic	Bands 6, 7, and 9 of sericite	Phyllic	Band 6	Band 7	Band 9		Yellow pixels represent argillic-phyllic alteration, green pixels represent phyllic alteration, and blue pixels represent propylitic alteration in the area (Fig. 3f)
			Pc1	0.7091	0.6366	0.3030		
			Pc2	0.6890	-0.7168	-0.1063		
			Pc3	-0.1495	-0.2842	0.9470		
	Argillic	Bands 5, 6, 7, and 8 of Kaolinite	Argillic	Band 5	Band 6	Band7	Band 8	
			Pc1	0.5751	0.5536	0.4925	0.3465	
			Pc2	0.3706	0.4746	-0.7110	-0.3629	
			Pc3	-0.7266	0.6833	0.0694	0.0154	
			PC4	0.0619	0.0348	0.4969	-0.8648	
	Propylitic	Bands 4, 6, 8, and 9 of Alunite	Propylitic	Band 4	Band 6	Band8	Band 9	
			Pc1	0.9469	0.2563	0.1595	0.109710	
			Pc2	0.3191	-0.8152	-0.4178	-0.242531	
			Pc3	-0.0329	-0.5185	0.7597	0.390828	

Method	Alternation	RGB (-PC4, PC3, PC6)							Description
PCA	Phyllic, Argillic, Propylitic	Eigenvector	Band 4	Band 5	Band 6	Band 7	Band 8	Band 9	Yellow pixels represent argillic-phyllic alteration, green pixels represent phyllic alteration, and blue pixels represent propylitic alteration in the region (Fig. 3g)
		PC1	0.8926	0.25384	0.2426	0.2148	0.1513	0.1039	
		PC2	0.4354	-0.33354	-0.4058	-0.5848	-0.3897	-0.2009	
		PC3	0.1076	-0.46251	-0.6163	0.5605	0.2663	0.0976	
		PC4	0.0421	-0.76401	0.6296	0.0919	-0.0492	-0.0844	
		PC5	-0.0013	-0.16095	0.0050	-0.5200	0.6200	0.5649	
		PC6	-0.0146	-0.02794	0.0047	0.1366	-0.6060	0.7829	

Spectrum based

Method	Alternation	Color of alternation area in map	Description
SAM	Phyllic	Green	Image obtained from the monitored classification with the SAM method that was carried out on images of Crosta (Fig. 3h)
	Argillic	Red	
	Propylitic	Blue	

3.2. Geo-chemical layers

3.2.1. Stream sediment data

According to the 1:25,000 topographic maps of the KB area, a total of 537 stream-sediment samples were collected from a -80 mesh grain size in a systematic network with a density of 7 samples per km^2 (Figure 3a). Each sample in every sampling location consisted of 20 sub-samples that were collected along between 30-m and 50-m from the drainage channel. The samples were prepared by sieving them 80 μm mesh size during the field surveys and then pulverized to < 200-mesh size in the laboratory. The samples were digested in HNO_3 + HCl (aqua region), and then analyzed for the 44 major and trace elements by Inductively Coupled Plasma-Optical Emission Spectrometry (ICP-OES) at the Amdel laboratory in Australia.

After pre-processing the raw geo-chemical data (e.g. detection of the censored data and replacing, correcting the out of order values, normalization), the statistical studies were carried out on the 44 elements in order to calculate the descriptive statistics of the geo-chemical data in the KB area (Table 2) and the statistical charts containing the histogram and q-q plots (Figures 4a, b). This data shows the non-normalized data and the possible existence of the Cu-Mo anomaly in the KB area. After normalizing the data, multivariate statistical processing such as cluster analysis (Figure 5), the Pearson correlation matrix (Table 3) and factors analysis (Table 4) were conducted on the data. These processes depicted the most important trace elements of the porphyry deposits (including Cu and Mo), having the highest correlation in comparison with the other elements. As shown in Table 4, the value correlation number for Cu and Mo is 0.58.

Based on Table 4, the elements are categorized into 9 paragenetic groups, which illustrate the possible existence of Cu-Mo. According to the fourth factor, the studied area has an association with the porphyry mineralization type. Concerning Table 4 and factor 4, Cu and Mo gained the most values (0.693 and 0.828, respectively), which could approve the existence of the porphyry deposit in the studied area. The results of cluster analysis (Figure 5) show that Cu and Mo are concentrated in one sub-group, and therefore, it may imply the existence of a possible porphyry deposit in the KB area.

Cheng *et al*. (1994) [47] have proposed an element concentration-area (CA) model, which was used to define the geo-chemical background and anomalies, utilized to separate the anomalies from the background. Considering the conceptual model of the porphyry deposits and the results obtained from the statistical studies, 4-element evidential layers (e.g. Cu, Mo, Te, Bi) from the stream sediment data were prepared (Figures 6a-h).

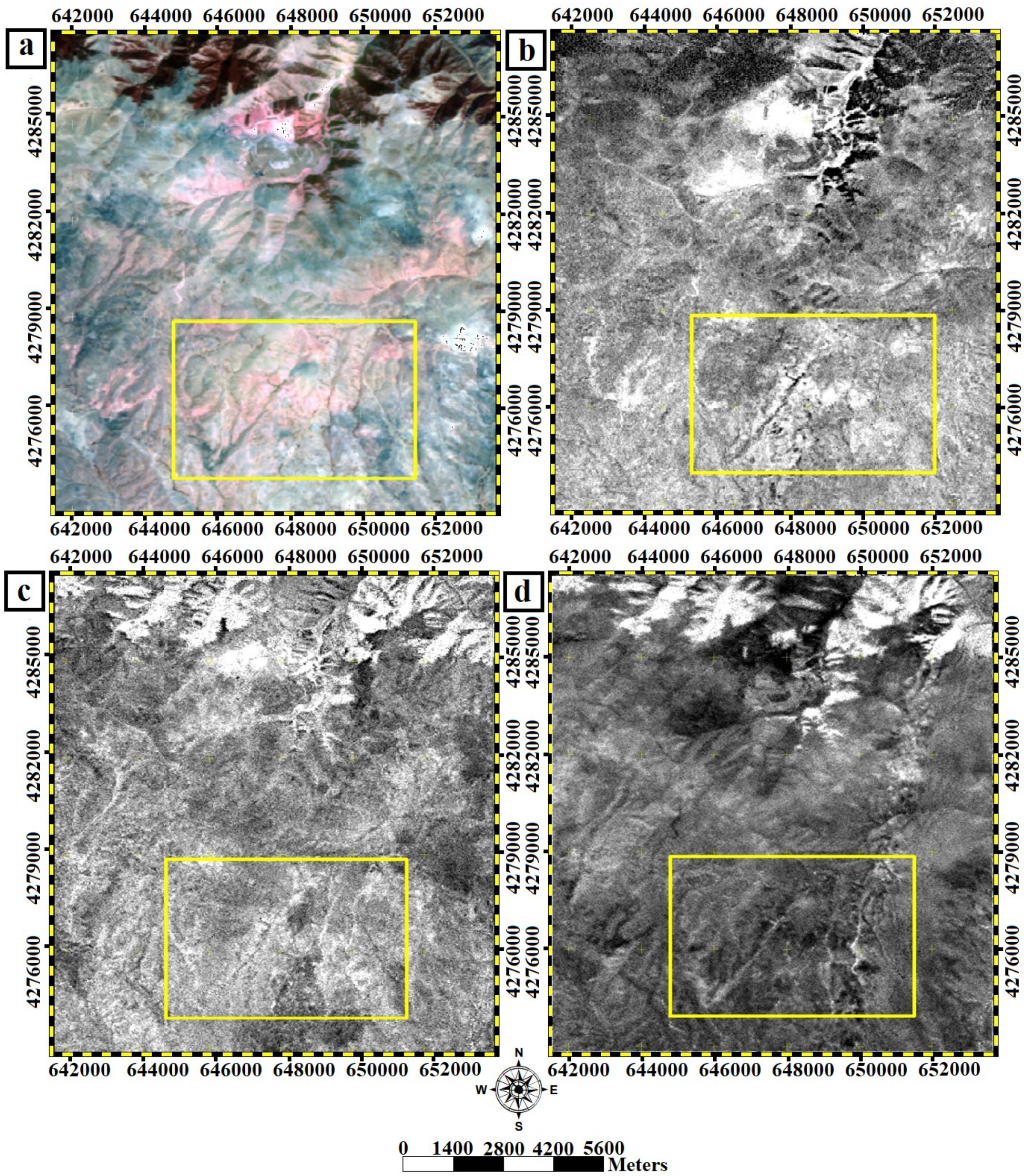

Figure 2. ASTER image processing of RGB composite colors of band ratios for (a) phyllic, (b) argillic, (c) propylitic alteration zones in KB area.

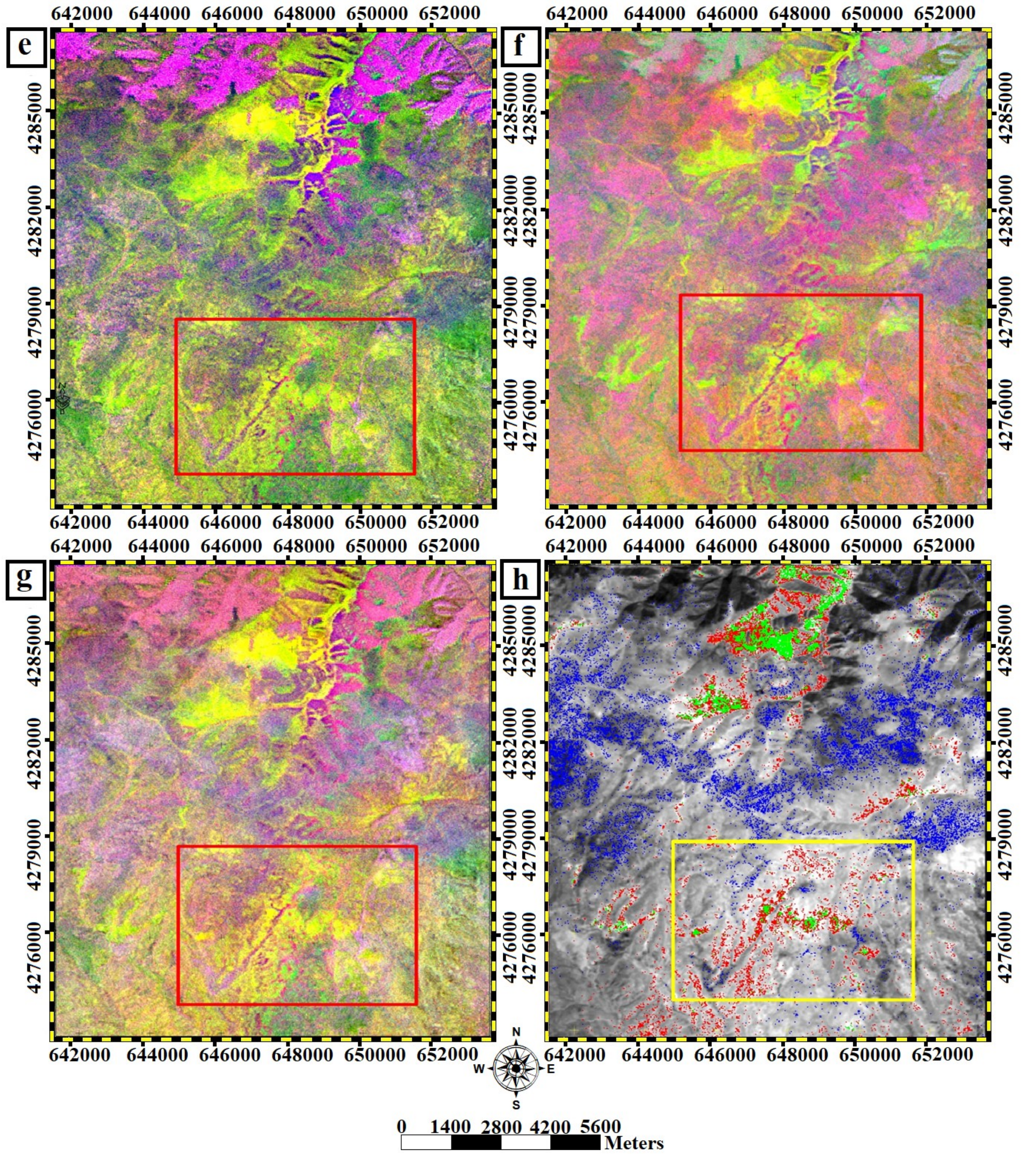

Continuation of Figure 2. ASTER image processing of RGB composite colors of band ratios for the (e, f) PCA, (g) Crosta, and (h) SAM techniques.

Table 2. The statistical characteristics of stream sediment geochemical trace elements in the KB area.

N	Range	Minimum	Maximum	Mean	Std. De.	Variance	Skewness	Kurtosis
As	69.6	0.4	70.0	15.7	0.4	97.1	2.2	7.6
Au	89.3	0.8	90.0	9.5	0.6	206.8	4.0	18.3
Bi	2.9	0.1	3.0	0.3	0.0	0.1	5.4	50.6
Cu	293.80	16.20	310.0	70.18	57.78	3338.87	2.76	7.69
Mo	18.9	0.1	19.0	3.6	3.4	11.5	2.3	5.7
Pb	400.5	9.5	410.0	64.6	3.3	5949.8	2.9	8.6
Sb	54	0.6	6.0	2.3	1.2	1.3	1.3	1.6
Te	1.9	0.2	2.0	0.3	0.0	0.0	2.8	11.7
Zn	860.0	40.0	900.0	152.43	150.54	22663.02	3.196	10.795

Table 3. Pearson correlation matrix of stream sediment geochemical trace elements in KB area.

	Ag	As	Au	Bi	Cu	K	Mn	Mo	Pb	Rb	Re	Sb	Sn	Te	W	Zn
Ag	1.00															
As	0.39	1.00														
Au	0.40	0.31	1.00													
Bi	0.03	0.12	0.27	1.00												
Cu	0.29	0.19	0.33	0.45	1.00											
K	0.23	0.07	0.19	0.16	0.10	1.00										
Mn	0.22	0.28	0.27	-0.01	0.13	0.16	1.00									
Mo	0.10	0.14	0.25	0.59	0.58	0.23	-0.03	1.00								
Pb	0.43	0.40	0.49	0.17	0.25	0.37	0.51	0.13	1.00							
Rb	0.14	0.01	0.07	0.18	0.05	0.84	0.06	0.25	0.18	1.00						
Re	0.10	0.04	0.02	-0.04	0.10	0.03	0.14	-0.01	0.06	-0.07	1.00					
Sb	0.35	0.41	0.38	0.19	0.12	0.43	0.24	0.34	0.58	0.34	-0.03	1.00				
Sn	-0.04	-0.01	-0.05	0.02	0.04	-0.04	0.03	0.01	-0.15	0.13	-0.01	-0.15	1.00			
Te	0.07	0.23	0.25	0.67	0.33	0.09	0.01	0.56	0.18	0.07	0.05	0.28	-0.04	1.00		
W	-0.16	0.06	0.05	0.26	-0.04	0.23	-0.07	0.36	0.14	0.25	-0.06	0.36	-0.09	0.19	1.00	
Zn	0.38	0.40	0.43	0.12	0.20	0.26	0.54	0.03	0.85	0.04	0.07	0.45	-0.17	0.12	0.17	1.00

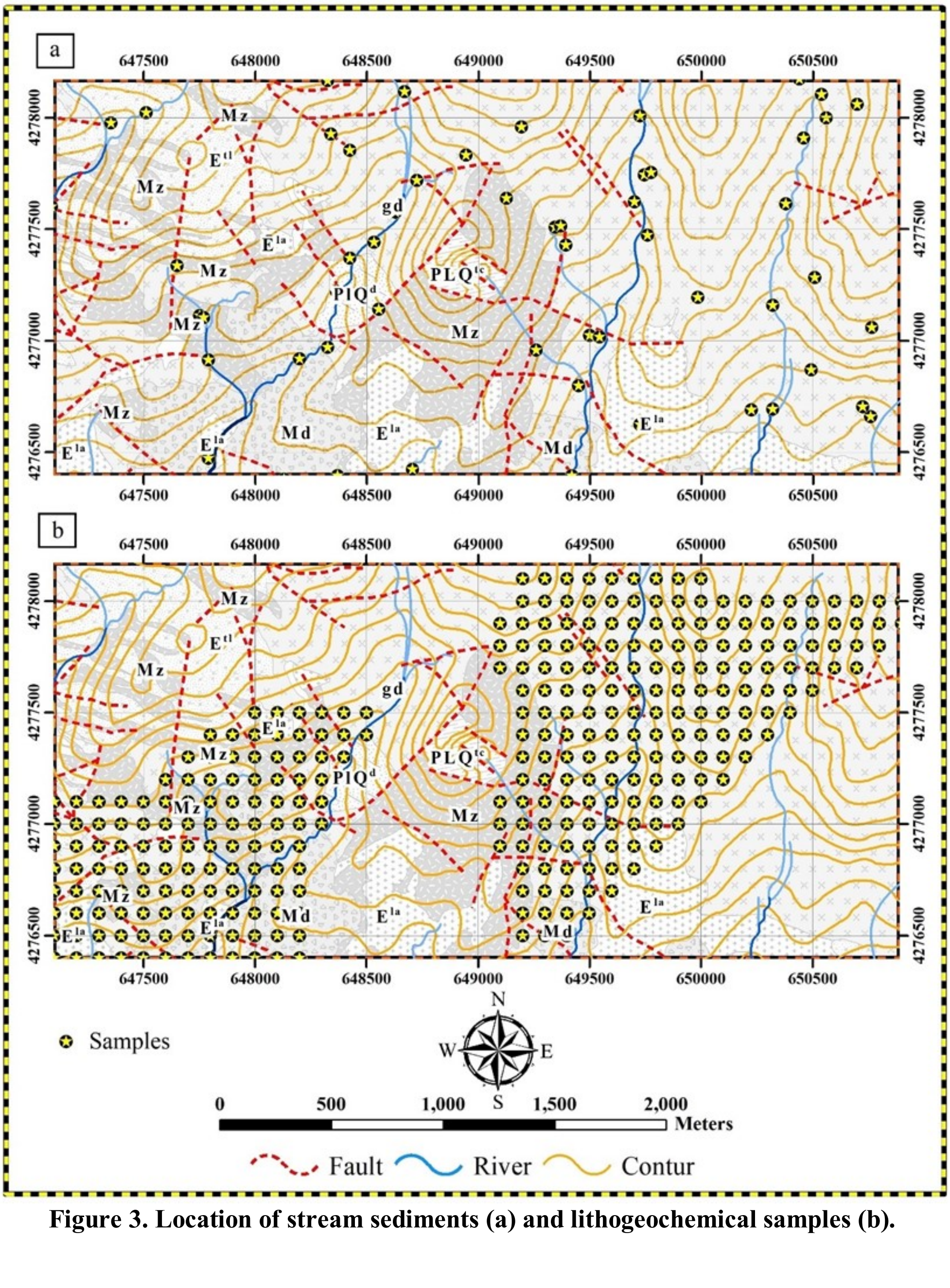

Figure 3. Location of stream sediments (a) and lithogeochemical samples (b).

Table 4. Factor analysis for multi-element geo-chemical data, where factor 4 corresponds to the Cu-Mo mineralization.

	Factor 1	Factor 2	Factor 3	Factor 4	Factor 5	Factor 6	Factor 7	Factor 8	Factor 9
Ag	-0.385	0.492	-0.044	0.17	0.026	0.015	0.272	0.083	-0.023
Al	-0.037	0.113	0.279	-0.138	0.279	0.296	-0.085	0.606	-0.141
As	-0.036	0.465	0.112	0.236	0.204	-0.033	0.473	0.089	0.006
Au	-0.14	0.57	-0.03	0.307	-0.008	0.111	0.1	0.132	-0.102
Ba	0.385	0.606	-0.064	-0.092	-0.064	-0.174	-0.158	0.327	0.239
Be	0.512	0.035	-0.198	-0.021	-0.219	0.436	0.268	0.429	0.012
Bi	0.246	0.136	-0.044	0.713	-0.177	0.257	-0.107	-0.011	-0.036
Ca	-0.219	0.198	0.08	-0.168	0.756	0.077	-0.017	-0.213	0.128
Cd	-0.25	0.815	0.128	0.132	-0.138	0.089	0.133	0.002	0.151
Ce	0.862	-0.094	-0.085	0.137	0.038	0.229	-0.112	-0.015	-0.126
Co	-0.138	0.121	0.637	0.356	-0.313	0.193	-0.096	0.059	0.05
Cr	0.143	-0.032	0.228	0.076	0.158	0.763	-0.007	0.187	-0.051
Cs	0.183	0.208	0.055	-0.184	0.01	0.008	0.778	-0.022	-0.113
Cu	-0.184	0.168	0.18	0.693	-0.06	0.044	-0.139	0.242	-0.024
Fe	-0.086	0.122	0.888	0.124	0.139	0.107	0.057	0.094	0.025
Hg	0.047	-0.106	0.102	0.008	0.065	-0.065	0.174	0.284	-0.579
K	0.049	0.436	-0.136	0.025	-0.678	-0.225	-0.061	-0.195	0.129
La	0.837	-0.138	-0.14	0.049	-0.036	0.243	-0.038	0.274	-0.001
Li	-0.362	0.188	0.216	-0.035	0.318	0.63	0.289	-0.097	0.023
Mg	-0.13	0.034	0.619	-0.153	0.193	0.515	-0.266	-0.04	-0.056
Mn	-0.188	0.497	0.539	-0.071	-0.217	0.111	0.046	0.099	0.103
Mo	0.189	0.074	-0.082	0.828	-0.177	-0.091	0.066	-0.045	-0.061
Na	0.36	-0.2	0.055	0.031	0.418	-0.099	-0.671	0.152	-0.043
Nb	0.813	-0.266	-0.117	-0.198	0.002	0.104	0.179	-0.244	0.101
Ni	0.343	0.111	0.145	0.141	0.122	0.808	-0.04	0.103	-0.003
P	0.62	-0.081	0.334	0.142	-0.085	-0.019	-0.172	0.352	0.026
Pb	-0.073	0.906	0.13	0.108	-0.054	-0.034	-0.036	-0.053	0.058
Rb	0.088	0.183	-0.123	0.059	-0.825	-0.115	0.108	-0.232	0.032
Re	-0.123	0.01	0.093	0.083	0.1	-0.035	0.099	0.133	0.721
S	-0.067	0.227	0.017	0.515	-0.077	-0.207	0.26	-0.086	0.325
Sb	0.05	0.612	-0.095	0.276	-0.132	-0.235	0.253	-0.259	-0.119
Sc	-0.224	-0.027	0.779	-0.148	0.097	0.263	0.211	0.044	-0.1
Sn	0.002	-0.245	0.173	0.02	-0.26	0.417	0.19	-0.117	0.055
Sr	0.387	-0.236	-0.064	-0.235	0.529	-0.038	-0.494	0.034	0.119
Te	0.136	0.113	-0.018	0.761	0.046	0.1	-0.068	-0.183	0.14
Th	0.868	-0.112	-0.331	0.039	0.003	0.033	-0.006	-0.029	-0.033
Ti	-0.06	0.399	0.477	-0.201	0.532	0.105	0.029	-0.229	0.147
nil	-0.294	0.531	-0.004	0.272	0.008	0.207	0.096	0.098	-0.374
U	0.859	-0.134	-0.224	0.091	-0.157	-0.064	0.048	0.041	-0.064
V	-0.117	0.11	0.889	-0.016	0.228	0.004	0.026	0.009	0.016
W	0.711	0.185	0.029	0.152	-0.057	-0.22	0.125	-0.335	-0.119
Y	0.174	-0.245	0.384	-0.154	0.028	0.412	0.407	0.105	0.354
Zn	-0.055	0.834	0.324	0.005	0.071	-0.015	0.044	-0.122	0.027
Zr	0.092	-0.129	0.018	-0.547	-0.091	0.195	0.553	-0.007	0.227

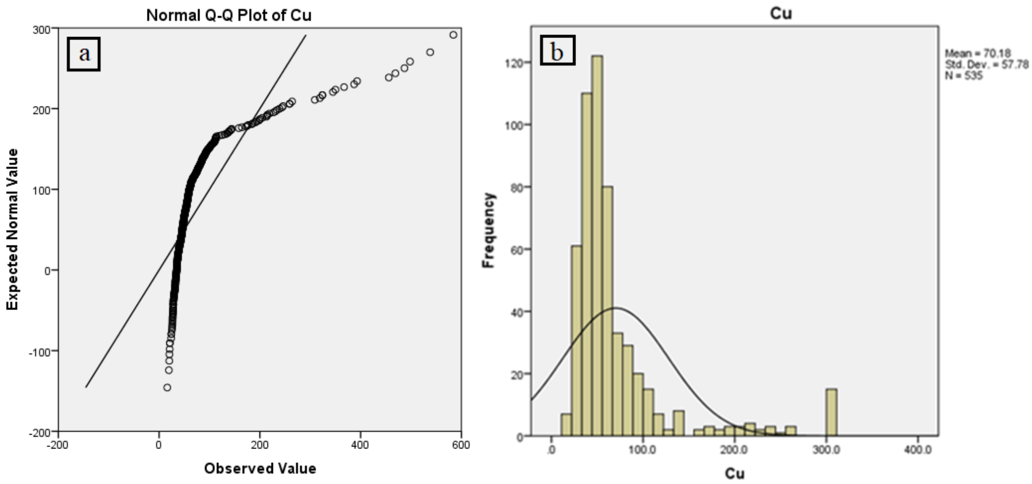

Figure 4. Statistical charts from stream sediment samples in KB area consisting of (a) Q-Q plots and (b) abundances histogram of elements.

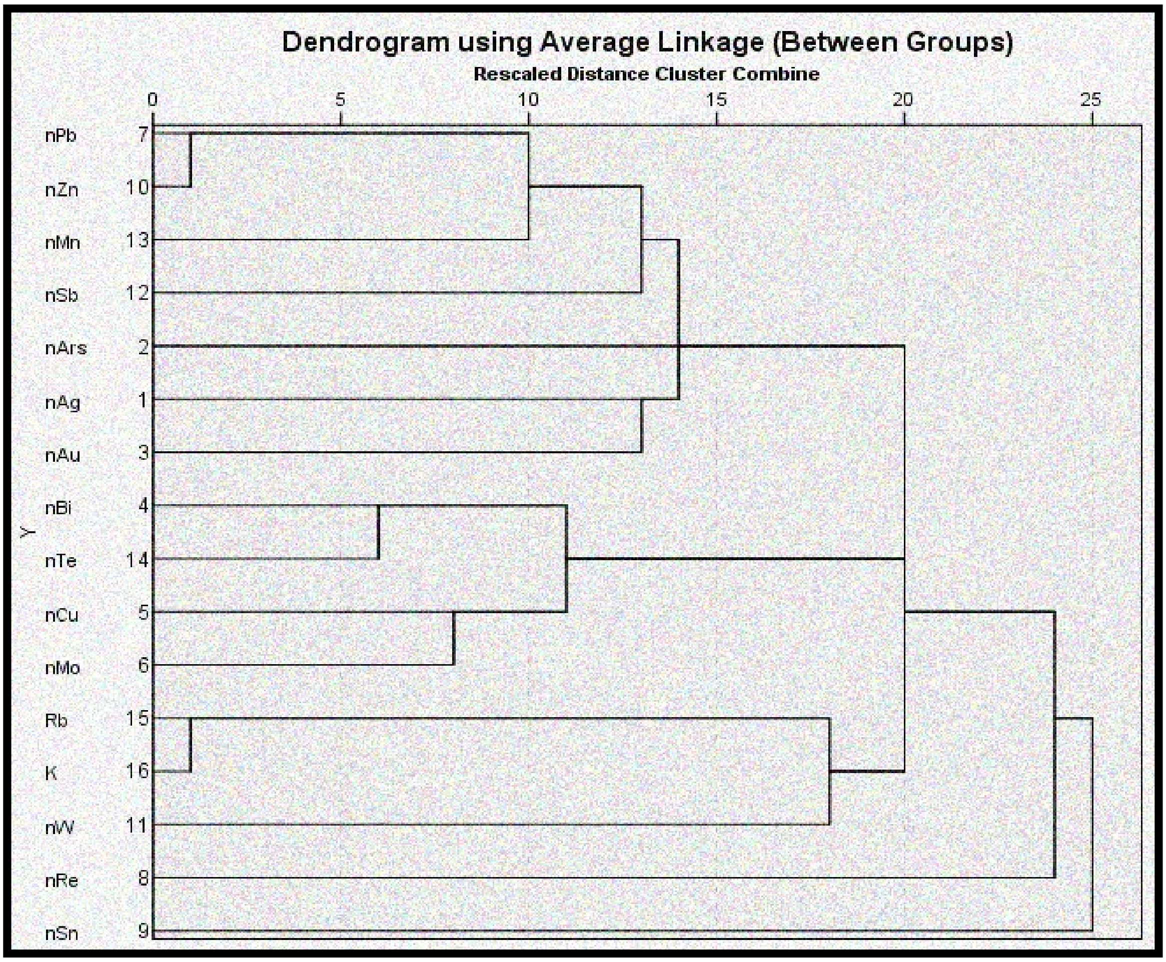

Figure 5. Cluster analysis of stream sediment data in KB area.

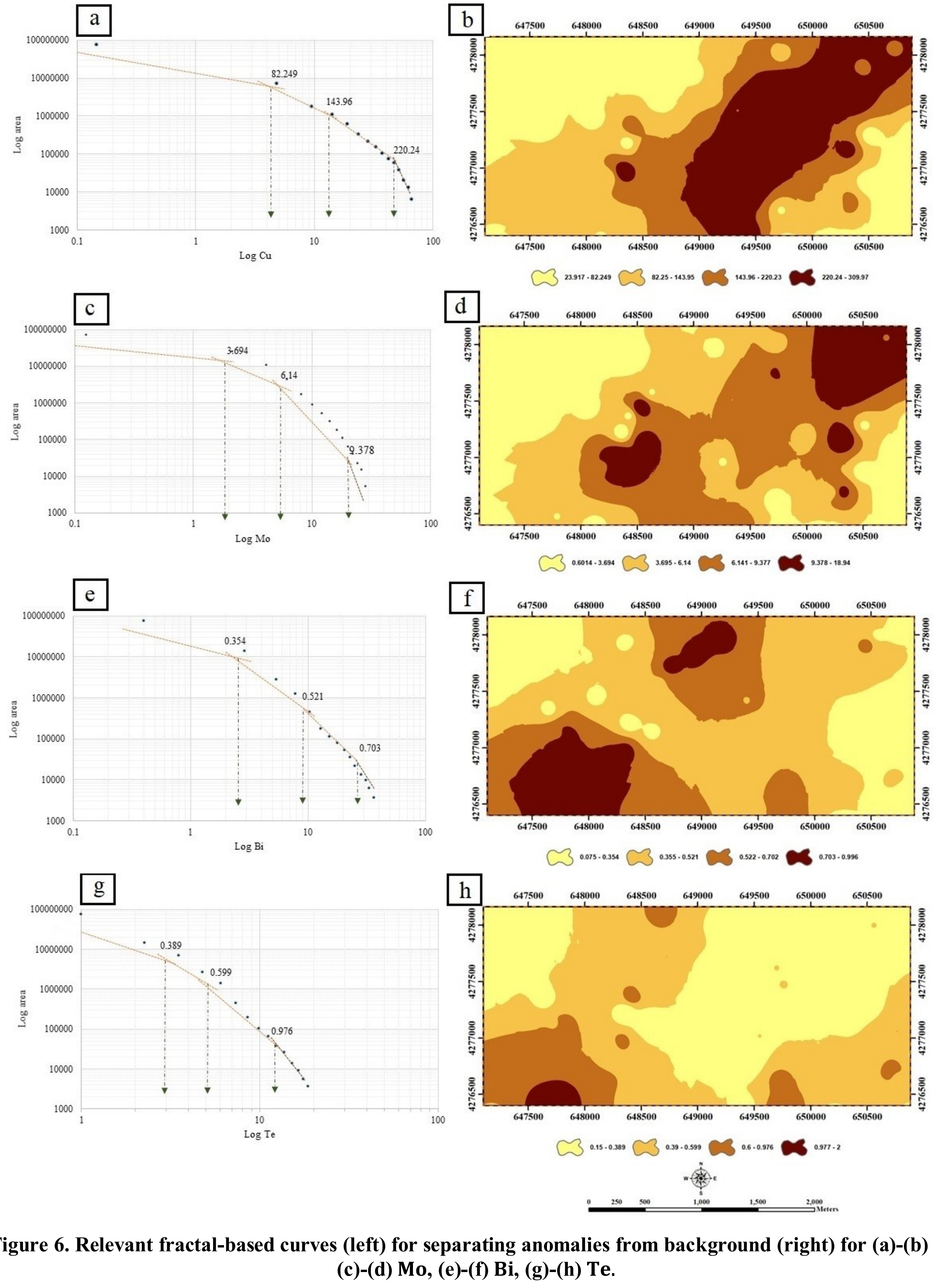

Figure 6. Relevant fractal-based curves (left) for separating anomalies from background (right) for (a)-(b) Cu, (c)-(d) Mo, (e)-(f) Bi, (g)-(h) Te.

3.2.2. Lithogeochemical data

A total of 205 lithogeochemical samples from the western and 303 lithogeochemical samples from the eastern parts of the studied area were collected in order to perform the geochemical studies of the alteration zones. The samples were crushed, reduced in volume, and pulverized to < 200-mesh size. The samples were digested in HNO_3/HCl (aqua region), and then analyzed using the Inductively Coupled Plasma Mass Spectrometry

(ICP-MS) for 44 elements at the Amdel laboratory, Australia.

3.2.2.1. Geo-chemical studies

All the pre-processing and processing methods including the detection of censored data and replacing, correcting the out-of-order values, normalization, and statistical processing were performed for the lithogeochemical data similar to the stream sediment samples (Figure 3b). The descriptive statistics of the lithogeochemical data in the KB area are present in Table 5, and the statistical charts (e.g. histogram) (Figure 7) illustrate the non-normalized data and the possible existence of the Cu-Mo porphyry deposit in the KB area. The Pearson correlation matrix (Table 6) with the value of 0.53 depicts the moderate correlation between Cu and Mo. The factor analysis (Table 7) was also carried out on the data. These processes also imply that Cu and Mo have the highest correlation in the area. Considering Table 7 and factor 3, Cu and Mo gained the most values (0.479 and 0.713, respectively), which could approve the existence of the porphyry deposit in the studied area. In addition, the cluster analysis (Figure 8) shows the existence of a possible porphyry deposit in the KB area.

The traditional methods were implemented on the lithogeochemical data for separating the geo-chemical anomalies from the background (Table 8). As mentioned earlier, considering the conceptual model of porphyry deposits and the results obtained from the statistical studies, 4-element evidential layers (e.g. Cu, Mo, Te, Bi) were selected to prepare MPM (Figures 9a-b).

Table 5. Statistical characteristics of lithogeochemical trace elements in KB area.

N	Range	Minimum	Maximum	Mean	Std. De.	Variance	Skewness	Kurtosis
As	114.6	8440.0	102900.0	11.0	14.0	197.2	3.9	19.4
Au	849.3	0.8	850.0	21.8	89.2	7953.5	7.6	61.9
Bi	7.7	0.1	7.8	0.4	0.6	0.4	6.5	59.7
Cu	2856.5	3.5	8260.0	106.4	31.6	79937.5	7.3	61.0
Mo	95.6	0.4	96.0	9.0	1.2	215.0	3.2	12.0
Pb	4949.9	0.2	495.0	138.9	512.3	262438.8	7.0	54.8
Sb	40.9	0.1	41.0	3.5	5.0	25.1	4.7	26.7
Te	2.85	0.15	3.00	0.2960	0.32285	0.104	4.002	21.824
Zn	2594.1	5.9	2600.0	148.30	300.3277	90196.713	4.836	28.150

Table 6. Pearson correlation matrix of lithogeochemical trace elements in KB area.

	As	Au	Bi	Cu	Fe	K	Mn	Mo	Pb	Rb	Re	Sb	Sn	Te	W	Zn
As	1.00															
Au	0.52	1.00														
Bi	0.39	0.46	1.00													
Cu	0.28	0.53	0.49	1.00												
Fe	0.26	0.28	0.25	0.45	1.00											
K	0.41	0.35	0.25	0.18	0.15	1.00										
Mn	0.09	0.01	-0.27	0.06	0.42	-0.03	1.00									
Mo	0.34	0.61	0.56	0.53	0.18	0.19	-0.27	1.00								
Pb	0.55	0.62	0.35	0.36	0.27	0.43	0.27	0.28	1.00							
Rb	0.39	0.38	0.30	0.16	0.09	0.82	-0.10	0.29	0.40	1.00						
Re	0.05	0.19	0.18	0.30	0.13	0.03	0.02	0.34	0.07	0.06	1.00					
Sb	0.68	0.56	0.41	0.32	0.22	0.40	0.07	0.46	0.62	0.43	0.10	1.00				
Sn	0.15	0.15	0.40	0.35	0.16	0.26	-0.37	0.42	-0.06	0.28	0.26	0.18	1.00			
Te	0.32	0.35	0.57	0.27	0.17	0.10	-0.17	0.43	0.23	0.14	0.12	0.30	0.19	1.00		
W	0.41	0.28	0.35	0.27	0.16	0.37	-0.09	0.37	0.18	0.42	0.23	0.44	0.40	0.24	1.00	
Zn	0.42	0.42	0.11	0.34	0.46	0.31	0.65	0.02	0.73	0.24	0.01	0.39	-0.15	0.06	0.04	1.00

Table 7. Factor analysis for multi-element geo-chemical data, where factor 3 corresponds to Cu-Mo mineralization.

	Factor 1	Factor 2	Factor 3	Factor 4	Factor 5	Factor 6	Factor 7	Factor 8
Al	0.407	0.375	-0.191	0.042	-0.019	-0.053	-0.666	-0.065
Ars	0.005	0.048	0.409	0.33	0.523	-0.087	0.289	-0.041
Au	-0.037	-0.303	0.566	0.233	0.42	0.184	0.116	0.117
Ba	0.05	0.021	-0.017	0.165	0.729	-0.122	-0.16	-0.078
Be	0.102	0.739	-0.039	-0.067	-0.072	-0.051	-0.109	-0.179
Bi	-0.013	-0.072	0.741	0.239	0.063	0.087	0.033	-0.207
Ca	0.238	0.13	-0.498	-0.595	0.001	0.075	0.041	0.223
Cd	0.142	-0.331	0.165	0.182	0.757	0.089	0.052	-0.009
Ce	0.24	0.807	-0.121	-0.045	-0.177	0.047	-0.01	0.045
Co	0.739	0.123	-0.353	-0.213	0.136	0.178	0.166	0.176
Cr	0.71	0.304	0.232	-0.082	-0.097	0.018	0.175	0.026
Cs	-0.171	0.107	0.053	0.597	0.027	0.008	-0.08	0.42
Cu	0.258	-0.235	0.479	0.068	0.179	0.443	0.148	-0.092
Fe	0.735	-0.152	0.24	0.083	0.26	0.101	0.018	-0.08
Hg	-0.022	0.047	0.039	0.045	0.014	0.63	0.146	-0.42
K	-0.012	-0.024	0.025	0.754	0.368	0.013	-0.129	-0.225
La	0.194	0.871	-0.123	-0.056	-0.151	0.034	-0.113	0.039
Li	0.151	-0.119	-0.141	-0.207	0.025	-0.023	0.071	0.7
Mg	0.814	0.082	-0.337	-0.172	0.111	0.06	-0.037	0.078
Mu	0.474	-0.016	-0.357	-0.204	0.587	0.108	0.13	0.238
Mo	-0.089	-0.177	0.713	0.253	-0.044	0.332	0.162	0.141
Na	0.188	0.417	-0.371	-0.502	-0.164	0.116	-0.166	0.018
NU	0.174	0.767	-0.286	-0.297	-0.062	-0.081	0.01	-0.016
Ni	0.63	0.416	-0.118	-0.203	-0.09	0.032	0.317	0.043
P	0.581	0.409	0.084	-0.279	-0.154	0.093	-0.131	0.006
Feb	-0.048	-0.202	0.324	0.202	0.804	0.017	-0.008	0.04
Rib	-0.087	-0.013	0.089	0.842	0.268	0.042	-0.106	-0.058
Re	0.095	0.077	0.227	0.07	-0.031	0.755	-0.111	0.197
S	-0.017	-0.062	0.676	0.171	0.172	0.183	-0.142	0.093
SU	-0.047	-0.044	0.415	0.423	0.472	-0.031	0.389	0.122
Sc	0.817	0.018	-0.049	0.058	0.107	-0.078	-0.271	0.066
Su	0.19	0.014	0.32	0.49	-0.351	0.29	0.009	-0.239
Sr	0.262	0.395	-0.38	-0.666	0.053	-0.03	-0.168	0.037
Te	0.006	0.066	0.713	0.023	0.073	-0.071	0.074	-0.104
Th	-0.075	0.883	-0.103	0.12	-0.098	0.01	-0.052	0.057
Ti	0.708	0.377	-0.214	-0.294	0.038	-0.064	-0.146	-0.033
T1	0.037-	0.024-	0.331	0.713	0.308	0.132	0.137	0.04-
U	0.027	0.826	0.128	0.157	0.067-	0.05	0.139	0.05-
V	0.845	0.016-	0.132	0.098	0.139	0.033-	0.202-	0.073-
W	0.089	0.338	0.297	0.524	0.078	0.208	0.331	0.125-
Y	0.488	0.282	0.482-	0.031	0.059-	0.156	0.198	0.264
Zu	0.293	0.256-	0.004-	0.061	0.842	0.072	0.044	0.024
Zr	0.084	0.347	0.53-	0.339-	0.046	0.237-	0.163-	0.036

Table 8. Calculations applied to separate anomaly from background by the traditional method.

	Cu	Mo	Bi	Te
X	106.4	9.04	0.39	0.29
S	282.65	14.66	0.64	0.32
X+S	389.06	23.70	1.03	0.62
X+2S	671.71	38.36	1.68	0.94
X+3S	954.36	53.02	2.32	1.26

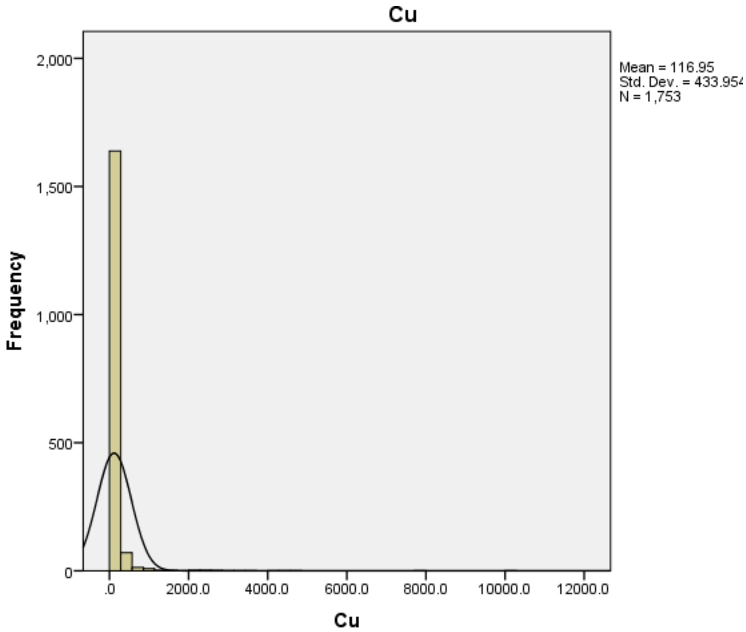

Figure 7. Statistical histogram of lithogeochemical samples in KB region.

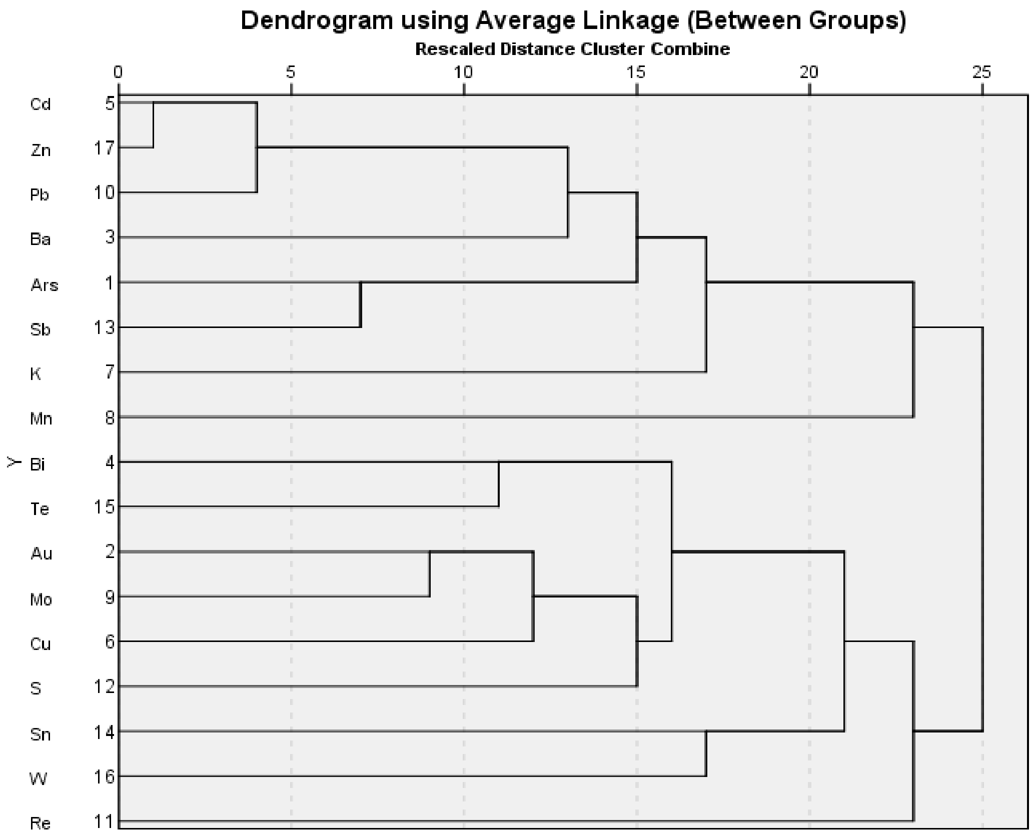

Figure 8. Cluster analysis of lithogeochemical data in KB area.

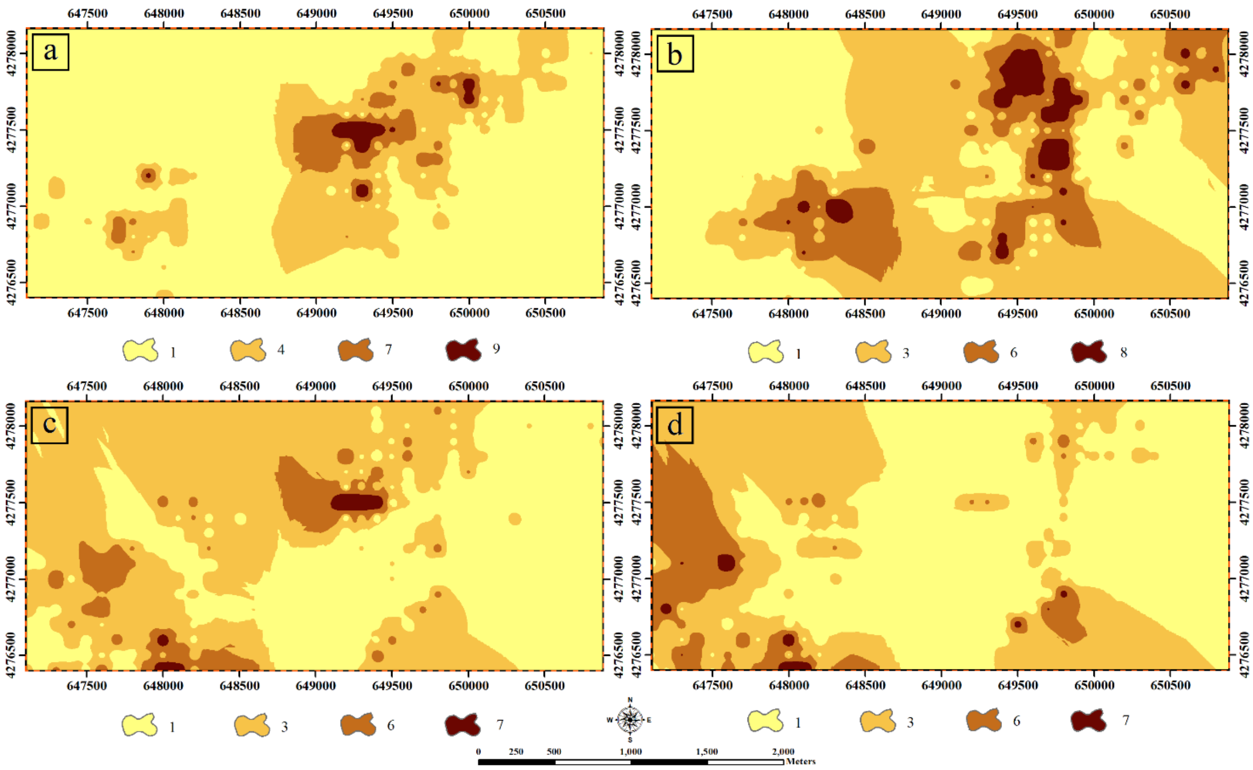

Figure 9. Separating anomalies from background by traditional methods for Cu (a), Mo (b), Bi (c), Te (d).

3.2.2.2. Hydrothermal alteration studies

3.2.2.2.1. Potassium alteration index

The potassic alteration zone spatially correlates to an increase in the potassium alteration index (Eq. 1) in the studied area and its adjacent areas. According to the diagram (Figure 10a) in potassic alteration, the amount of potassium has increased, and conversely, the abundance of sodium and calcium has decreased. Applying the oxide ratios of these elements, the areas with a high potassium alteration intensity can be identified [48].

$$K_2O/ (CaO + Na_2O) \qquad (1)$$

According to the map generated by the potassium index (Figure 10b), the north-western parts of the eastern area as well as the central and western parts of the western area show the highest values of the potassium alteration index. These areas can be distinguished by a white color.

3.2.2.2.2. Phyllic alteration index

As presented by Large *et al*. (2001) [48], an increase in the abundance of the phyllic (sericitic) alteration index (Eq. 2) can be correlated to the intensity of the phyllic alteration (Figure 10c). However, this index indicates a blind mineralization in the studied area.

$$K_2O/ (K_2O+Na_2O) \qquad (2)$$

The areas with the highest intensity of phyllic alteration zones are highlighted by white color (Figure 10d). In general, this index is very consistent with the potassic alteration. However, the haloes intensity in the phyllic alteration is almost lower than potassic, and the alteration haloes in the phyllic alteration are greater than the potassic zone.

3.2.2.2.3. Propylitic alteration index

This ratio is considered as the chlorite index (Eq. 3), and an increase in this ratio corresponds to an increase or intensity of chlorite alteration in the area (Figure 10e). This index is applied in the exploration of the blind Cu-Mo deposits [48].

$$((MgO+ FeO)/(MgO + FeO + K_2O + Na_2O))\times 100 \qquad (3)$$

According to Figure 10f, the chlorite alteration is shown in the areas where the potassic and phyllic alteration indices are low and the areas marked in dark colors are correlated to the lowest propylitic alteration index, which are also well-consistent with the potassic and phyllic alteration zones.

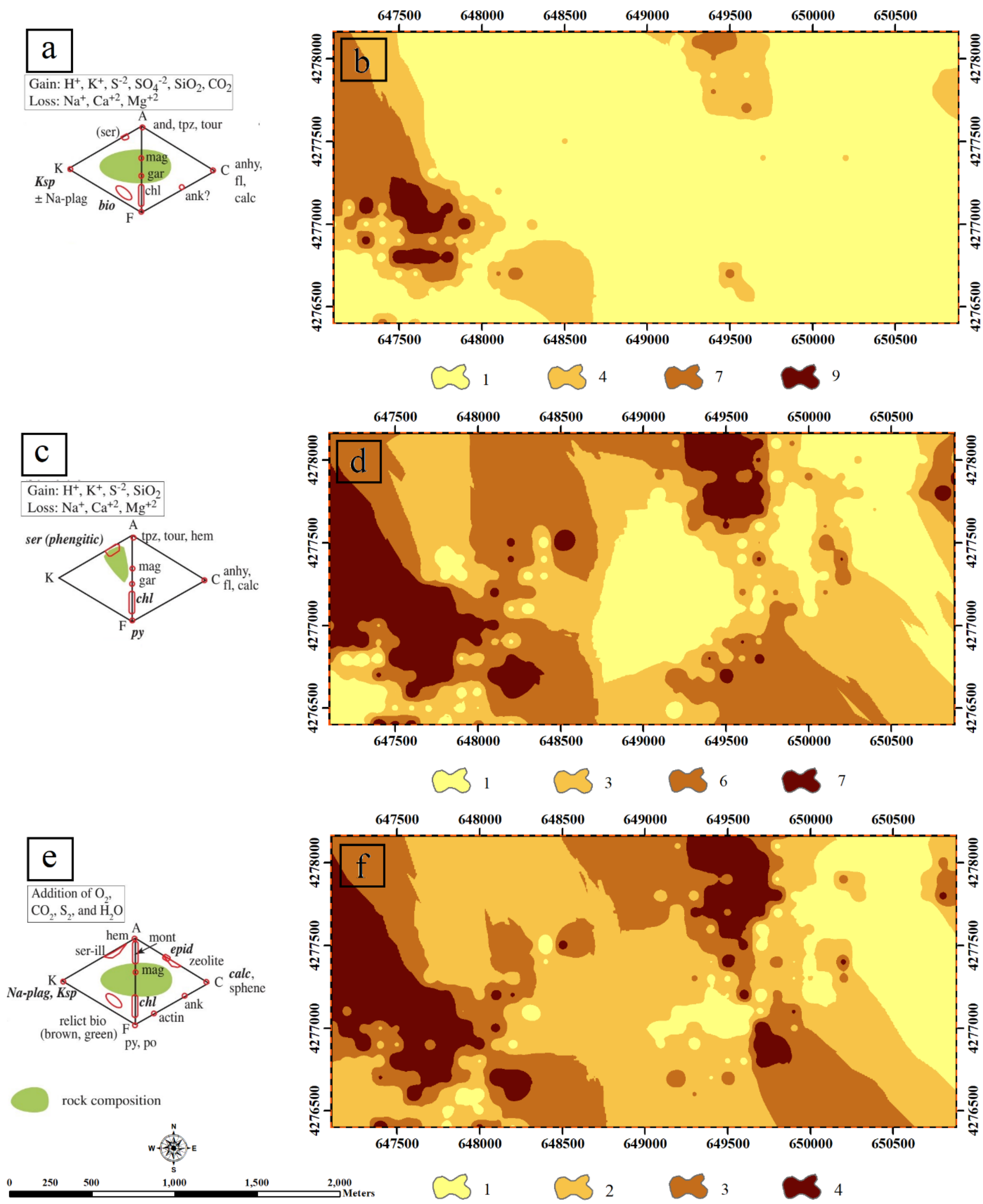

Figure 10. Left column presents AKF–ACF diagram (Meyer *et al.*, 1967) for alteration index maps in the right column, (a)-(b) potassic, (c)-(d) phyllic, (e)-(f) Bi, (g)-(h) propylitic.

3.2.3. Zonality indices of KB

Considering the porphyry Cu-Mo mineralization type in the KB deposit, the applied zonality indices were selected through to the porphyry copper deposit conceptual model. Afterward, the vertical geochemical zonation (Vz) models were performed based on the typical porphyry Cu-Mo deposits in Kazakhstan, Bulgaria, Armenia, and Iran [49].

Following the processing of the statistical parameters and associated variables of the paragenetic elements in the possible porphyry mineralization, two sets of halo variables were introduced in the area (Table 9). According to the obtained Vzs, the surface erosion maps for the stream sediments (Figures 11a, b) and lithogeochemical data (Figures 11c, d) were generated.

Table 9. Sets of halo variables in KB area.

	Supra-ore elements	Sub-ore elements	Vz
1.	Ba, Hg, Sb, As	Mo, Ni, Co, Bi	(Ba*Hg*Sb*As)/(Mo*Ni*Co*Bi)
2.	Pb, Zn	Cu, Mo	(Pb*Zn)/(Cu*Mo)

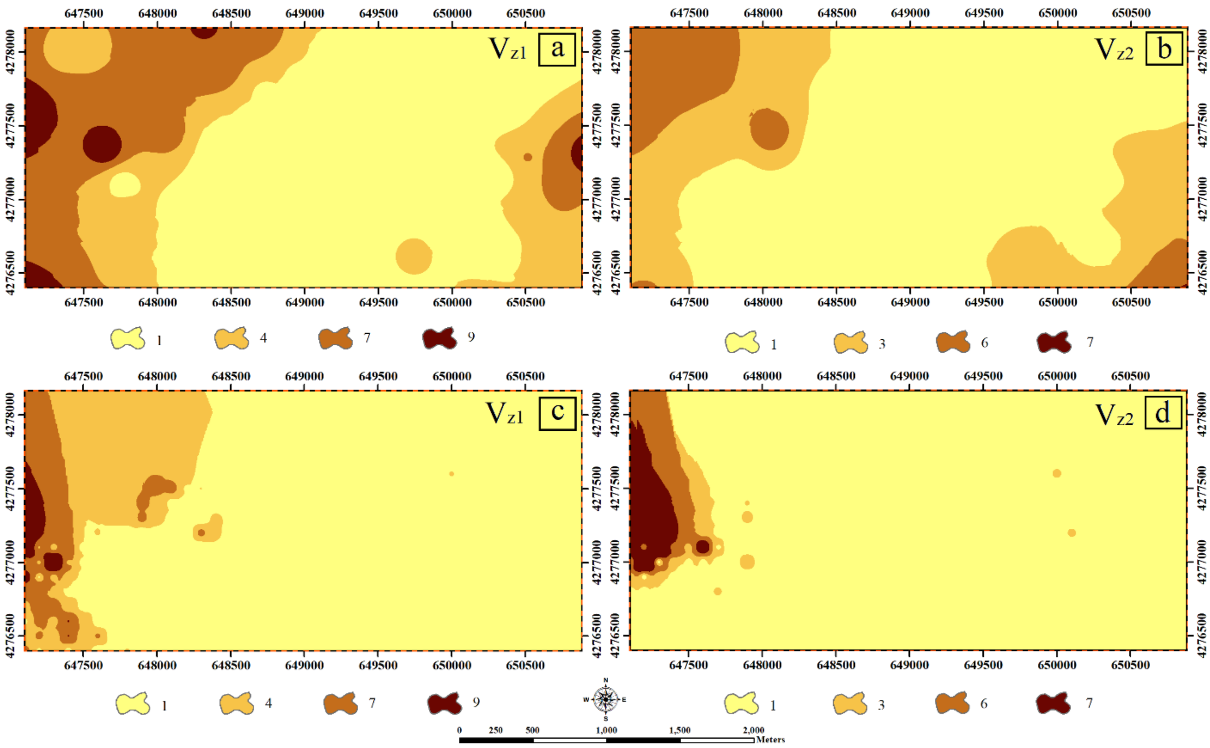

Figure 11. Surface erosion maps (V_{z1} and V_{z2}) for stream sediment (a, b) and lithogeochemical data (c, d).

3.3. Geological layer

The lithology and fault layers were fused and used in order to generate the geological layer. For assigning values to the lithology layer of the KB area, the importance of the host rocks in the porphyry copper deposit was considered (Figure 12a). Therefore, the granodiorite and monzonite units gained the most value. For the fault layer, the buffering was carried out on the faults, and a close distance was gained for most values (Figure 12b).

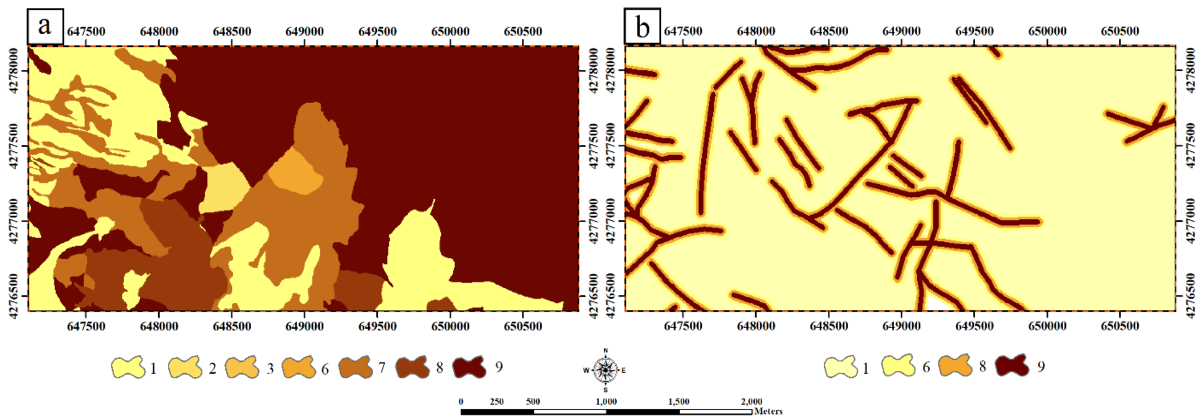

Figure 12. Evidential layers of (a) lithology and (b) faults.

3.4. Alteration layer

As investigated by KCE (2006) [40], the studied area includes different types of potassic alteration, phyllic, argillic, advanced argillic, propylitic, and silicified alteration haloes. Furthermore, according to remote sensing, the existence of the Cu-Mo porphyry alterations was verified. This layer was generated through scanning the alteration zones in both the geological and remote sensing layers and by utilizing the polygon drawing option (Figure 13a) in the ArcGIS software (version 10.8). In the final step, the weights assigned to the alteration zone were considered for the conceptual model of the porphyry copper systems (Figure 13b).

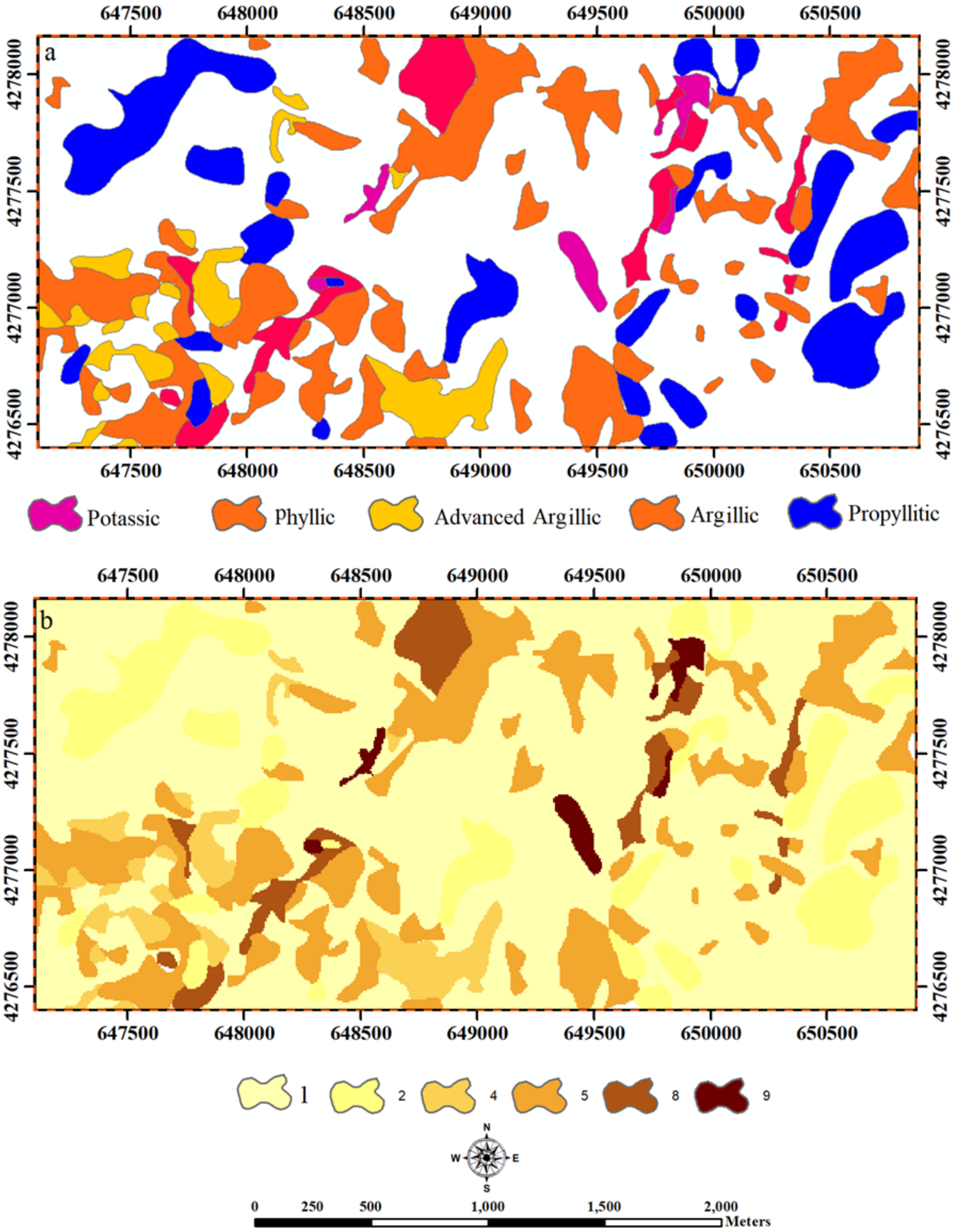

Figure 13. Alteration map (a) and evidential layer of alteration (b).

4. Geo-spatial datasets and MPM

The flowchart (Figure 14) describes all the utilized predictive layers extracted from the geo-chemical, lithology, and alteration data to generate MPM. The decision tree shown in Figure 14 illustrates the procedure of preparing the final fuzzy fusion map.

First, all the predictive layers were weighted based on importance and priority, and then the layers were fuzzified through large functions. In this function, the high-weighted areas in the fuzzy mode will also have high values. The weights assigned to the different areas of each layer were written in the legend section of the evidential layers.

According to Figure 14, the flowchart consists of three main branches that are integrated by gamma-operator including geo-chemistry, alteration, and lithology. The geo-chemistry and lithology branches have two sub-branches integrated by the OR operator. The stream-sediment and lithogeochemical layers were created through the integration of their sub-branches through the AND operator.

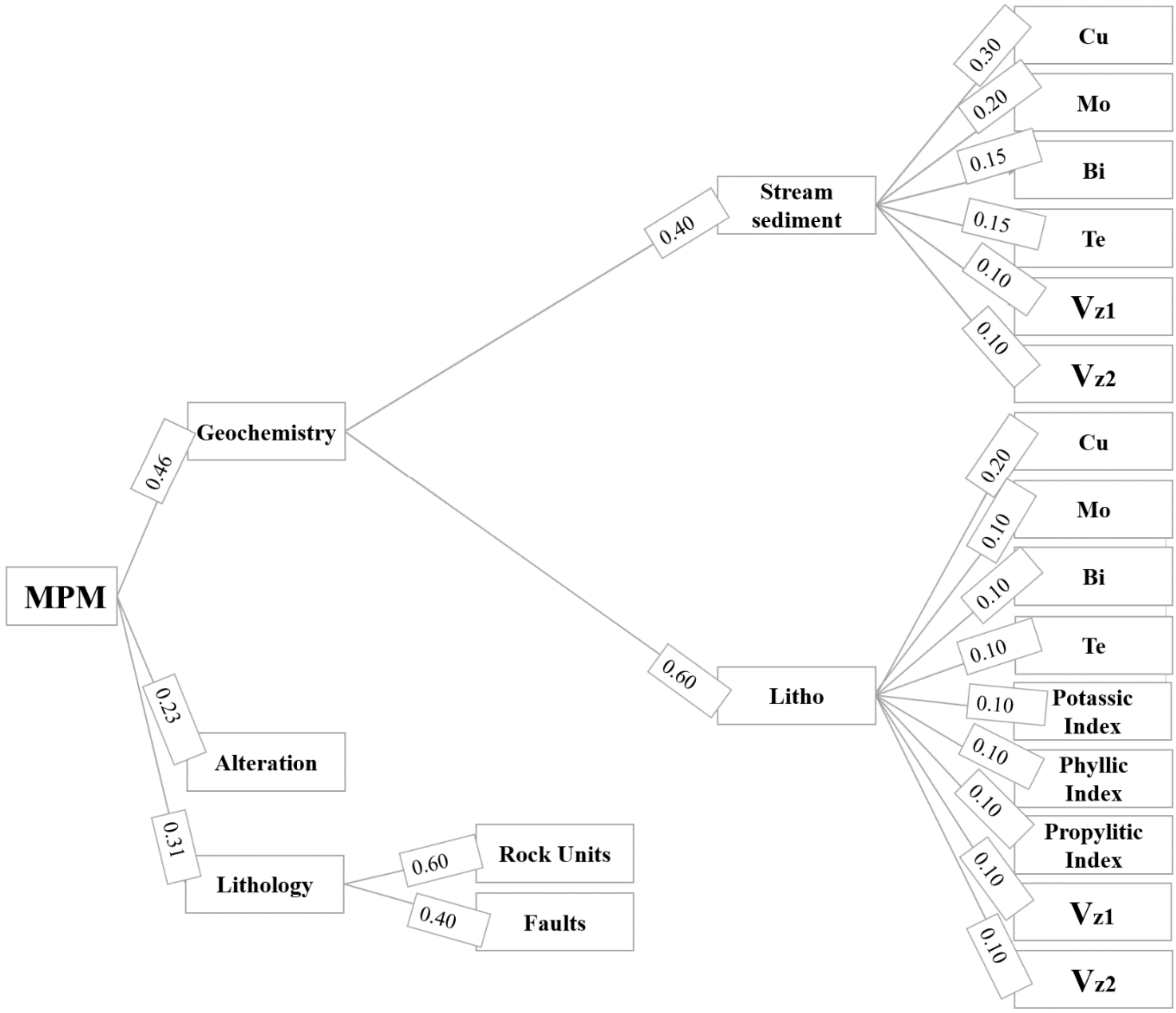

Figure 14. Decision tree flowchart for generating final prospectivity map.

As presented by Zadeh (1965) [5], the fuzzy set denotes a continuous scale from 0 to 1 replaced with the theory of false or true (0 or 1). There is no limitation on choosing the fuzzy membership weights; the selection of the value (weighting of evidence) is gained entirely by the geo-expert [50].

Among the fuzzy algebraic operators that have been widely investigated [5,51], the fuzzy gamma operator approach lets for the more pliable fusion of weighted maps, and could be readily implemented with the ArcGIS software. For the KB area, the gamma value was defined through the trial-and-error technique that was equivalent to 0.83, and it was utilized to combine the layers to create MPM (Figure 15).

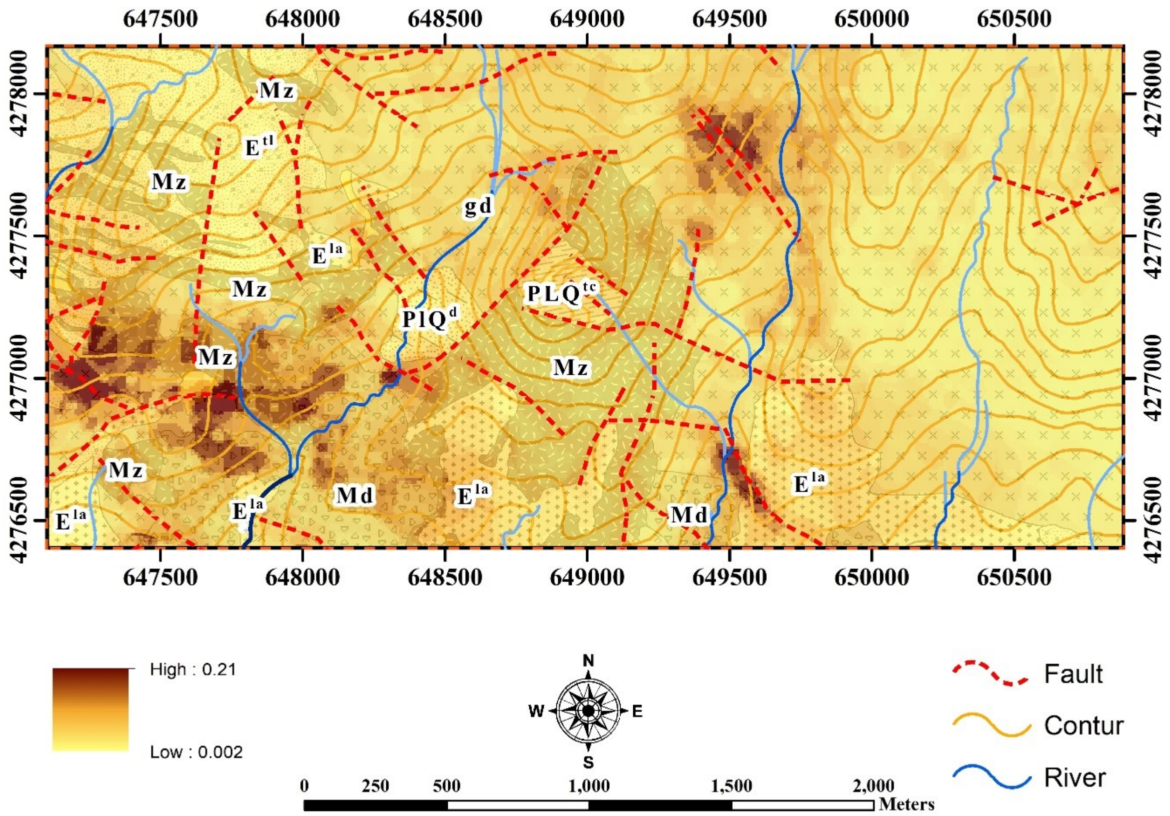

Figure 15. Final mineral potential mapping of KB area.

5. Discussion and conclusions

The present investigation integrated the geological, alteration, and geo-chemical data in order to prepare MPM in the KB Cu-Mo porphyry deposit. By fusion of the rock units and fault layers, the geological layer was generated. The remote sensing and geological studies were applied in order to generate the alteration layer. For creating the geo-chemistry layer, the stream-sediment and lithogeochemical data was employed. This study was suggested using the new criteria layers for assessing the potential area. Applying the surface erosion layers can provide acceptable results in the MPM layers. The lithogeochemistry layer was categorized into 9 layers including Cu, Mo, Bi, Te, and the alteration indices (e.g. potassic, phyllic, and propylitic) and zonality indices (e.g. V_{z1} and V_{z2}). In addition, the stream-sediment layer was categorized into 6 layers including Cu, Mo, Bi, Te, and the zonality indices (e.g. V_{z1} and V_{z2}). By examining the created layers, the consistency of the potential areas was verified by field surveys. Afterward, the weights were assigned to each layer considering the conceptual model of the porphyry copper systems. Consequently, the layers were integrated by the fuzzy gamma operator technique, and the final MPM was generated. In the final MPM, 72181.4 m^2 of the area under study (0.86% of the studied area) had a high potential, and these areas were proposed for further exploration drilling locations.

In addition, regarding the remote sensing, geo-chemical, and geological studies performed in the KB areas, the categorized results can be drawn as follows:

5.1. Mineralization in eastern and south-eastern Kighal

The total area for the altered and mineralized zones in the eastern and south-eastern parts of Kighal is approximately 5 Km^2. As illustrated by KCE (2006) [40], the rock units cropped out in this zone consists mainly of Eocene to Oligocene PlQ^{tc} (andesitic to trachy-andesitic lava flows and dome), O^{ag} (intercalations of agglomerate, brecciated tuff, and trachy-basaltic lava flows), E^{tb} (trachy-basalt to basaltic andesite lava flows interbedded with purple to gray tuff), E^{b} (alternations of andesitic, basaltic andesite and basaltic lava flows), O^{tc} (intercalations of thin- to medium-bedded trachy-andesite, tuff, and agglomerate) intruded by Oligocene to Miocene

Mz (porphyritic to micro-porphyritic monzonite, monzodiorite, and quartz monzonite intrusive bodies) with the north-south direction. The altered and mineralized zone is intersected by the north-south trending andesite and latite-andesite dikes as well as the faults with different strikes. In addition, the argillic, advanced argillic, propylitic, and silicified zones comprise the main hydrothermal alterations in the area.

Considering the remote sensing studies, the phyllic and argillic alteration zones have not been significantly developed in this zone, and the propylitic alteration has been poorly observed in the area. The results obtained from the remote sensing studies correlated with the field surveys [40].

The geo-chemical indices obtained indicated the weak occurrence of propylitic alteration in the studied area. Furthermore, the characteristics and index trace elements of porphyry copper mineralization were distinguished in the area. Therefore, the results of the lithogeochemical data processing did not show any significant anomalies of element enrichment associated with the porphyry copper deposit. Based on the zonality indices, this zone consists of a moderate level of erosion.

Finally, the results of the fuzzy fusion studies demonstrated a weak potential for the porphyry copper mineralization in the area.

5.2. Mineralization in north-eastern part of Kighal

The altered and mineralized zones in the north-eastern part of the Kighal area are primarily characterized by the volcanic to sub-volcanic flows intruded by granodiorite to monzonite porphyry intrusive bodies. This area developed in 2.5 Km^2 consists mainly of Eocene to Oligocene O^r (rhyolitic and rhyodacitic dome), E^{tb} (intercalations of purple to gray trachy-basaltic and basaltic andesite lava flows), E^{la} (porphyritic andesite to latite lava flows), intruded by Oligocene to Miocene Mz (propyritic to micropropyritic monzonite, monzodiorite and quartz monzonite), gd (porphyritic granodiorite to monzodiorite), and Md (propyritic micro-granodiorite to micro-monzonite intrusive bodies. The main alteration zones in this area include the potassic, phyllic, argillic, advanced argillic, propylitic, and silicified zones. This zone is considered as the main altered and mineralized zone that extends to a large area over the Jyjrchay River and the surrounding valleys. Several late- to post-mineralization andesite, latite, rhyolite, monzonite, monzonite to granodiorite dikes with different strikes crosscut the altered and mineralized zone. Moreover, this zone is intersected by major northwest-southeast-trending faults.

According to the remote sensing studies, the phyllic and argillic alteration zones are well-developed but the propylitic alterations are very weakly observed in the area. The compliance of these results with the alteration map of the area [40] indicates the exploratory importance of the studied area.

The geochemical indices obtained indicate the strong presence of potassic and phyllic alteration in most outcrops. Based on the results obtained from the stream sediment data, strong anomalous elements containing copper, molybdenum, bismuth, and telluride exist in the studied area. These elements are considered as the trace elements of the conceptual model in the porphyry copper deposits. The presence of these trace elements (Cu, Mo, Te, Bi) was also demonstrated by the lithogeochemical data. According to the erosion level studies, this zone is affected by the severe and relatively deep level of erosion. It seems that the Jyjrchay River is considered as the most important factor during the erosion of mineralization of the area.

Finally, the results of the fuzzy fusion studies are indicative of having considerable potential in the terms of the porphyry type copper mineralization in north-eastern Kighal.

5.3. Mineralization in central part of Kighal Bourmolk

This mineralization and alteration zone with 3 Km^2 of the area is located in the central part of the studied area. The hydrothermal alterations in this area are extensive and varied (e.g. potassic, argillic, advanced argillic, phyllic, propylitic, and silicification). The rock units cropped out in this area consist of porphyritic micro-granodiorite to micro-monzonite (md), porphyritic granodiorite to monzodiorite (gd), porphyritic to micro-porphyritic monzonite, monzodiorite and quartz monzonite (mz) porphyritic andesitic, latitic lava flows (E^{la}), and monzonite. The area is primarily affected by the intrusive bodies ranging from granodioritic to micro-monzonitic and monzonite in composition. The faults in this area are generally characterized by a northwest-southeast trend, and near the vertical dip that is correlated to the strike of late dikes. Furthermore, the quartz veins are more developed in this area.

Based on the remote-sensing studies, the phyllic and high-intensity argillic alteration zones can be observed in the area. The considerable consistency of the remote-sensing results with the alteration zones presented by KCE (2006) [40] indicates the exploratory importance of the area. The geo-chemical studies illustrate the strong presence of potassic and phyllite alterations in this area. The results of the stream sediment and lithogeochemical data indicated strong anomalies of the elements involving Cu, Mo, Bi, and Tl in the area. Considering the zonality indices, this zone is superimposed by a severe and deep-level of erosion.

The results of fuzzy fusion demonstrated a considerable potential for porphyry-type copper mineralization in the studied area. The mineralization pattern of this area is significantly consistent with the central part of KB.

5.4. Mineralization in Bourmolk area

The Bourmolk alteration and mineralization zone with an area of 6 Km^2 is located in the western part of the studied area. The volcanic flows and pyroclastic units consist of green tuff (E^t), intercalation of green tuff, andesitic, latite lava flows (E^{tl}), and intercalation of purple tuff and andesitic flows (E^{ta}). These country rocks are intruded by monzonite and dacite intrusive bodies that result in the formation and development of the phyllic, argillic, advanced argillic, and propylitic alteration zones.

The remote-sensing studies indicate that the argillic and high-intensity propylitic alteration zones are well-developed in this area. According to the stream sediment and lithogeochemical investigation, strong anomalies of Au, Pb, Zn, As, Cd, Mn, Sb, and Sn trace elements typical for the epithermal-type Au-Ag mineralization were distinguished in this area. Considering the erosion level studies, this area only shows a weak and shallow level of erosion, and therefore, any outcrops of phyllic and/or potassic alteration zones could not be observed in this area. The results of the layer integration indicate a high potential of exploration for the gold-silver epithermal mineralization at the near-surface and shallow levels, and porphyry Cu-Mo mineralization at deeper levels.

Acknowledgments

We would like to thank the staff of the National Iranian copper industries company (NICICO), for permitting us to have access to the analysis of stream sediments and the lithogeochemical samples. The authors gratefully acknowledge the Editor-in-Chief, Associate Editor, and two anonymous reviewers of the Journal of Mining and Environment for their constructive reviews.

References

[1]. Abedi, M. and Norouzi, G.H. (2012). Integration of various geophysical data with geological and geo-chemical data to determine additional drilling for copper exploration. Journal of Applied Geophysics, 83, 35-45.

[2]. Barak, S., Abedi, M., and Bahroudi, A. (2020). A knowledge-guided fuzzy inference approach for integrating geo-physics, geo-chemistry, and geology data in a deposit-scale porphyry copper targeting, Saveh, Iran. Bollettino di Geofisica Teorica ed Applicata. 61(2).

[3]. Bonham-Carter, G.F. (2014). Geographic information systems for geo-scientists: modeling with GIS (Vol. 13). Elsevier.

[4]. Carranza, E.J.M. (2008). Geo-chemical anomaly and mineral prospectivity mapping in GIS. Elsevier.

[5]. Zadeh, L. A. (1965). Information and control. Fuzzy sets. 8 (3): 338-353.

[6]. Barak, S., Bahroudi, A., and Jozanikohan, G. (2018). Exploration of Kahang porphyry copper deposit using advanced integration of geological, remote sensing, geo-chemical, and magnetics data. Journal of Mining and Environment. 9 (1): 19-39.

[7]. Khalifani, F., Bahroudi, A., Barak, S., and Abedi, M. (2019). An integrated Fuzzy AHP-VIKOR method for gold potential mapping in Saqez prospecting zone, Iran. Earth Observation and Geomatics Engineering. 3 (1): 21-33.

[8]. An, P. (1991). Application of fuzzy set theory to integrated mineral exploration. Can. J. Explor. Geophys., 27, 1-11.

[9]. Bonham-Carter, G.F. (1994). Geographic information systems for geoscientist-modeling with GIS. Computer methods in the geo-scientists, 13, 398.

[10]. Knox-Robinson, C. M. (2000). Vectorial fuzzy logic: a novel technique for enhanced mineral prospectivity mapping, concerning the orogenic gold mineralization potential of the Kalgoorlie Terrane, Western Australia. Australian Journal of Earth Sciences, 47(5), 929-941.

[11]. Barak, S., Imamalipour, A., Abedi, M., Bahroudi, A., and Khalifani, F.M. (2021). Comprehensive modeling of mineral potential mapping by integration of multiset geo-sciences data. Geo-chemistry. 81 (4): 125824.

[12]. Porwal, A., Das, R. D., Chaudhary, B., Gonzalez-Alvarez, I., & Kreuzer, O. (2015). Fuzzy inference

systems for prospectivity modeling of mineral systems and a case-study for prospectivity mapping of surficial Uranium in Yeelirrie Area, Western Australia. Ore Geology Reviews, 71, 839-852.

[13]. Barak S., Bahroudi A., and Jozanikohan G. (2018b): The use of fuzzy inference system in the integration of copper exploration layers in Neysian, Iran. J. Min. Eng., 13, 21-35.

[14]. Pan, G. and Porterfield, B. (1995). Large-scale mineral potential estimation for blind precious metal ore bodies. Nonrenewable resources. 4 (2): 187-207.

[15]. Porwal, A., Carranza, E.J.M., and Hale, M. (2003). Artificial neural networks for mineral-potential mapping: a case study from Aravalli Province, Western India. Natural resources research. 12 (3): 155-171.

[16]. Porwal, A., Carranza, E.J.M., and Hale, M. (2004). A hybrid neuro-fuzzy model for mineral potential mapping. Mathematical Geology. 36 (7): 803-826.

[17]. Bonham-Carter, G.F. and Chung, C.F. (1983). Integration of mineral resource data for Kasmere Lake area, North-west Manitoba, with emphasis on uranium. Journal of the International Association for Mathematical Geology. 15 (1): 25-45.

[18]. Bonham-Carter, G.F., Agterberg, F. P., and Wright, D.F. (1989). Integration of geological datasets for gold exploration in Nova Scotia. Digital Geologic and Geographic Information Systems, 10, 15-23.

[19]. Carranza, E. J. M. and Hale, M. (2002). Where are porphyry copper deposits spatially localized? A case study in Benguet province, Philippines. Natural Resources Research. 11(1): 45-59.

[20]. Agterberg, F. P. and Bonham-Carter, G.F. (1999, October). Logistic regression and weights of evidence modeling in mineral exploration. In Proceedings of the 28th international symposium on applications of computer in the mineral industry (APCOM), Golden, Colorado (Vol. 483, p. 490).

[21]. Ghaeminejad, H., Abedi, M., Afzal, P., Zaynali, F., and Yousefi, M. (2020). A fractal-based outranking approach for mineral prospectivity analysis. Bollettino di Geofisica Teorica e Applicata. 61 (4): 555-588.

[22]. Panahi, S., Khakzad, A., and Afzal, P. (2021). Analytical hierarchical prospectivity mapping using the integration of exploratory data in the Anarak region, Central Iran. Geopersia.

[23]. Shahbazi, S., Ghaderi, M., and Afzal, P. (2021). Prognosis of gold mineralization phases by multi-fractal modeling in the Zehabad epithermal deposit, NW Iran. Iranian Journal of Earth Sciences. 13 (1): 31-40.

[24]. Jackson, R. G. (2010). Application of 3D geochemistry to mineral exploration. Geochemistry: Exploration, Environment, Analysis. 10 (2): 143-156.

[25]. Imamalipour, A. and Mousavi, R. (2018). Vertical geochemical zonation in the Masjed Daghi porphyry copper-gold deposit, north-western Iran: implications for exploration of blind mineral deposits. Geochemistry: Exploration, Environment, Analysis. 18 (2): 120-131.

[26]. Aliyari, F., Yousefi, T., Abedini, A., and Calagari, A.A. (2021). Primary geo-chemical haloes and alteration zoning in the primary geo-chemical haloes and alteration zoning applied to gold exploration in the Zarshuran Carlin-type deposit, north-western Iran. J. Geoch. Explor. 231, 1-19.

[27]. Solovov, A.P. (1987). General prospecting for mineral deposits. Mir, Moscow.

[28]. Wang, C., Carranza, E. J. M., Zhang, S., Zhang, J., Liu, X., Zhang, D., and Duan, C. (2013). Characterization of primary geo-chemical haloes for gold exploration at the Huanxiangwa gold deposit, China. Journal of Geochemical Exploration, 124, 40-58

[29]. Imamalipour, A., Karimlou, M., and Hajalilo, B. (2019). Geo-chemical zonality coefficients in the primary halo of Tavreh mercury prospect, north-western Iran: implications for exploration of listwaenitic type mercury deposits. Geochemistry: Exploration, Environment, Analysis. 19 (4): 347-357.

[30]. Aliyari, F., Afzal, P., Lotfi, M., Shokri, S., and Feizi, H. (2020). Delineation of geo-chemical haloes using the developed zonality index model by multivariate and fractal analysis in the Cu–Mo porphyry deposits. Applied Geochemistry, 121, 104694.

[31]. Bazin, D. and Hubner, H., (1969). Copper deposits in Iran, Geological survey and mineral exploration of Iran.

[32]. NICIC; National Iranian Copper Industries Co. (1989). Investigating copper deposits in the northern region of East-Azarbaijan. Kansaran Engineering Consulting.

[33]. Karimi, M. (1989). Summary of Studies on Copper Deposits in North-East Azerbaijan, Ministry of Mines and Metals, National Iranian Copper Industries Co.

[34]. Stöcklin, J. (1968). Structural history and tectonics of Iran: a review. AAPG Bulletin. 52 (7): 1229-1258.

[35]. Nabavi, M. (1976). An introduction to the geology of Iran, Geological Survey of Iran Publication.

[36]. Hassanpour, S., Alirezaei, S., Selby, D., and Sergeev, S. (2014). SHRIMP zircon U-Pb and biotite and hornblende Ar-Ar geochronology of Sungun, Haftcheshmeh, Kighal, and Niaz porphyry Cu–Mo systems: evidence for an early Miocene porphyry-style mineralization in northwest Iran. Int J Earth Sci 104:45–59.

[37]. Jamali, H. and Mehrabi, B. (2015). Relationships between arc maturity and Cu–Mo–Au porphyry and related epithermal mineralization at the Cenozoic Arasbaran magmatic belt. Ore Geology Review, 65, 487-501.

[38]. Moritz, R., Johannes, M., Maria, O., Dave, S., Massimo, Ch., Nino, P., Vladimer, G., Ramaz, M., Rafael, M., Rodrig, T., Arman, V., Samvel, H., Vagif, F., and Mamoy, M. (2011). Major Cu, Au, and Mo deposits of the Lesser Caucasus: products of diverse geodynamic settings. Swiss Geoscience Meeting, Symposium 2: Mineralogy–Petrology–Geochemistry, 2. 16, pp. 3–4.

[39]. Ghorbani, M. (2013). The Economic Geology of Iran: Mineral Deposits and Natural Resources, Springer Scientific Publication, 569 pp.

[40]. KCE; Kavoshgaran Consulting Engineers, (2006). The report of geological and alteration studies in Kighal-Bourmolk, National Iranian Copper Industries Co.

[41]. Sillitoe, R. (2010). Porphyry Copper Systems, Society of Economic Geologists, Inc. Economic Geology, 105, p. 3-41

[42]. Rajendran, S., Thirunavukkarasu, A., Balamurugan, G., and Shankar, K. (2011). Discrimination of iron ore deposits of granulite terrain of Southern Peninsular India using ASTER data. Journal of Asian Earth Sciences. 41(1): 99-106.

[43]. Abrams, M. J., Brown, D., Lepley, L., and Sadowski, R. (1983). Remote sensing for porphyry copper deposits in southern Arizona. Economic Geology. 78 (4): 591-604.

[44]. Ghulam, A., Amer, R., and Kusky, T.M. (2010). Mineral exploration and alteration zone mapping in the Eastern Desert of Egypt using ASTER Data. In ASPRS 2010 annual Conference.

[45]. Alavi Panah, K. (2003). Application of Remote Sensing in Earth Sciences, University of Tehran.

[46]. Munyati, C. (2004). Use of principal component analysis (PCA) of remote sensing images in wetland change detection on the Kafue Flats, Zambia. Geocarto International. 19 (3): 11-22.

[47]. Cheng, Q., Agterberg, F. P., and Ballantyne, S.B. (1994). The separation of geo-chemical anomalies from the background by fractal methods. Journal of Geochemical Exploration. 51 (2): 109-130.

[48]. Large, R.R., Gemmell, J.B, and Paulick, H. (2001). The alteration box plot: a simple approach to understand the relationship between alteration mineralogy and lithogeochemistry associated with volcanic-hosted massive sulfide deposits, Economic Geology, 96, p. 957-971.

[49]. Ziaii, M., Carranza, E.J.M., and Ziaei., M. (2011). Application of geochemical zonality coefficients in mineral prospectivity mapping, Computers and Geosciences. 37, np. 1935-1945.

[50]. Nykänen, V. and Salmirinne, H. (2007). Prospectivity analysis of gold using regional geo-physical and geo-chemical data from the Central Lapland Greenstone Belt, Finland. Geological Survey of Finland, 44, 251-269.

[51]. Lee, S. (2007). Application and verification of fuzzy algebraic operators to landslide susceptibility mapping. Environmental Geology, 52 (4): 615-623.

استفاده از عملگر فازی گاما در تهیه نقشه پتانسیل معدنی برای کانسارهای مس- مولیبدن پورفیری (مطالعه موردی: ناحیه کیقال-بارملک)

مسعود اسمعیل زاده[۱]، علی امامعلی پور[۱*] و فرهنگ علیاری[۲]

۱- بخش مهندسی معدن، دانشگاه ارومیه، ارومیه، ایران
۲- بخش مهندسی معدن دانشگاه صنعتی ارومیه، ارومیه، ایران

ارسال ۲۰۲۱/۰۹/۲۰، پذیرش ۲۰۲۲/۰۳/۰۷

* نویسنده مسئول مکاتبات: a.imamalipour@urmia.ac.ir

چکیده:

هدف اصلی اکتشاف ذخایر معدنی کشف نهشته‌های کانساری است. روش‌های تهیه نقشه پتانسیل معدنی (MPM) با استفاده از تصمیم گیری چند معیاره (MCDM) لایه‌های اکتشافی را تلفیق می‌کنند. این کار تحقیقاتی، داده‌های زمین شناسی، دگرسانی و ژئوشیمیایی را به منظور تولید MPM در محدوده کانسار مس- مولیبدن پورفیری کیقال- بارملک تلفیق می‌کند. برای تهیه لایه زمین شناسی، از هم پوشانی لایه‌های واحدهای سنگی و گسل‌ها استفاده شد. از روش دورسنجی و مطالعات زمین شناسی برای تهیه لایه دگرسانی استفاده شد. برای تولید لایه ژئوشیمی از داده‌های رسوبات آبراهه‌ای و لیتوژئوشیمیایی استفاده شد. لایه لیتوژئوشیمی به تعداد نه لایه شامل لایه‌های Te, Bi, Mo, Cu، اندیس‌های دگرسانی (برای مثال پتاسیک، فیلیک و پروپلیتیک)، واندیس‌های منطقه‌بندی ژئوشیمیایی (برای مثال V_{z1} and V_{z2}) تقسیم شد. فزون بر آن، لایه رسوبات آبراهه‌ای به شش لایه شامل لایه‌های Te, Bi, Mo, Cu و اندیس‌های منطقه بندی ژئوشیمیایی (برای مثال V_{z1} and V_{z2}) تقسیم شد. با بررسی لایه‌های ایجاد شده، سازگاری مناطق پتانسیل توسط بررسی‌های میدانی تایید شد. سپس، با در نظر گرفتن مدل مفهومی سیستم‌های مس پورفیری، وزن‌ها به هر لایه اختصاص داده شد. در نتیجه، لایه‌ها با روش عملگر فازی گاما تلفیق شد و MPM تولید گردید. با توجه به MPM تولید شده، ۰/۸۶ درصد از منطقه مورد مطالعه پتانسیل کانی سازی پورفیری بالایی را نشان می‌دهد و این مناطق برای مکان‌های حفاری اکتشافی بعدی پیشنهاد می‌شود.

کلمات کلیدی: تهیه نقشه پتانسیل معدنی، مس- مولیبدن پورفیری، عملگر فازی گاما، کانی سازی، کیقال- بارملک.